Chapter 3

Homogeneity and fractality
Luca Amendola

Homogeneity and Fractality
Luca Amendola

Abstract. I review the controversial issue of large scale inhomogeneity in the galaxy distribution. The common statistical estimators of clustering, like the power spectrum, assume that the surveys from which the estimation is made are much larger than the scale of homogeneity. However, I argue that the evidence that this is so is at best only indirect, and depends on the specific model of structure formation. If the current surveys are still below the homogeneity scale, as a close examination of the main redshift surveys indicates, the galaxy distribution can be approximated by a fractal. I review the statistics of fractals and show that it is useful to understand the large scale structure. In particular, the large variance of fractals forces to discard the use of the clustering amplitude, e.g. the amplitude of the power spectrum, and to focus the investigation on the trend of the clustering with scale.

In the last Chapter I present an inflationary model of structure formation that may produce large scale inhomogeneity without violating the cosmic microwave constraints.

3.1 Introduction

3.1.1 Fractals and real world

The universe is certainly not homogeneous, and very likely is not a fractal. Then, why should we bother with distributions which are homogeneous or fractal? The reason is that to make any progress in studying raw data we need models, and the two simplest models for distributing particles in space are the homogeneous and the fractal one. In the first case, the average number of particles in cells centered on particles, i.e. the number of neighbors, increases as r^3; in the fractal case, the increase is as r^D. Any other distribution requires more parameters to be characterized, and as such may be considered as "more complicated". Therefore, the properties of these simple distributions are indeed extreme, and their study is useful to investigate the limits within which the real world is located.

Let me state from the very beginning that these lectures are not meant to take a definite positions on the issue of what is the scale of homogeneity. First, because it is not the task of theorists to take positions, and in any case introductory lectures would not be the proper place to do so. Secondly, because I believe the data are still insufficient to establish even the simplest statistical estimator, the homogeneity scale, whatever its definition may be.

Rather than trying to draw conclusions, I have in mind two goals:

- to show that fractals are useful to investigate large scale structure even if the universe is homogeneous at some scale
- to show that the difference between the standard scenario of structure formation, the Cold Dark Matter (CDM) theory and its variants, and the fractals, is only quantitative, and not qualitative.

In other words, the task I proposed myself in writing these lectures was to find an unifying language between the mathematics of fractal and the standard cosmology. The main problem of doing so is that while the fractals are a mathematical object, cosmology speaks of physical processes taking place in space and time. Our universe had a finite time to evolve, and its initial conditions may be inferred from observations of the microwave background and of distant objects. The theory of fractals only knows distributions of particles, produced with abstract algorithms, static in time and possibly infinite in space. The only reason why fractals are of interest to the real world is that we see an inhomogeneous universe, with clusters and voids extending to tens or even hundreds of megaparsecs, and that any inhomogeneous distribution can be described, although only as a first approximation, as a fractal, or a finite portion of it. The link between real cosmology and abstract fractals is therefore that a fractal approximates, for small intervals of time and space, the real distribution of matter. How small the intervals are, can only be decided by observations.

It is important at this point to remark that the matter in our universe assumes many different forms. We can look at the luminous matter or at the total gravitational field; and if we study only the luminous matter, we can investigate infrared- or optically-selected galaxies, or bright galaxies, or clusters, and each class of object may exhibit different properties, for instance different level of inhomogeneities. As a consequence, the intervals in which a fractal approximates the real distribution can be larger, for instance, for clusters than for the total matter.

The lectures are divided in four parts. In the second chapter, I introduce most of the mathematics and statistics we need throughout. Particular emphasis will be put on the power spectrum, which I find the easiest way to speak of fractals to cosmologists, and of cosmology to the people who works with fractals in other areas. It is also the main product of most theories of structure formation and of observation campaigns, so that it embodies most of the knowledge we currently have about how the matter is distributed. In the third chapter I expose the predictions in terms of power spectrum of standard CDM theories and of fractals. We will see then that the power spectra of CDM and of (finite portion of) fractals look the same, except for the fact that the fractal spectrum always increases with the sample size, while the CDM spectrum do so only below the homogeneity scale. I will also show that the large variance of fractal models does not allow to use the amplitude of the power spectrum, or related quantities, as a test of fractality. Homogeneity and fractality can only be tested through the trend of clustering with the scale. In the fourth chapter I consider some observational data, from surveys as CfA, SSRS, Las Campanas, and argue that we are not yet convincingly above the homogeneity scale, so that the fractal properties of the CDM-like models can still bias our results. In the fifth chapter I leave the raw data and their analysis, and expose a model of structure generation that can produce large inhomogeneities at the present without conflicting with the main body of the standard cosmological scenario. I present it here in order to give an example of how a modest extension of the inflationary model can give a very different geography of the matter at the present time, more inhomogeneous and more non-gaussian.

In these lectures I focus on the information provided by the galaxy surveys. There are of course other important sources of information on the matter dis-

tribution in our universe, for instance from the cosmic microwave background or the X background or the Lyman-α clouds, but the link between these sources and the present large scale structure is certainly more indirect, and requires a stronger appeal to theoretical models.

3.1.2 Historical background

Although today the homogeneous and the fractal vision of the world tend to conflict head-on, it is interesting to note that their history began almost simultaneously. Maybe the first model of the universe based on a physical theory, Newton's law, rather than on pure speculation, was proposed by Newton himself in 1692 answering to some letters of Rev. Bentley on the cosmological properties of the gravitation's law. Newton proposed that the system of stars resists the gravitational collapse by virtue of specially arranged initial conditions: if all stars are equally spaced, by God intervention, then each star feels the same attraction in all directions, and therefore remain stable. In the following years, the model was made more precise: Newton proposed that all stars have equal intrinsic brightness, and that those of first magnitude lie equally spaced on a shell at unit distance from us, those of second magnitude lie similarly on a shell at double distance, and so on through the faintest stars. This models is clearly homogeneous averaging over a few unit distances, and also more or less accounts for the relative number of stars at various magnitudes.

Around 1750 Johann Heinrich Lambert proposes the first strongly inhomogeneous model, a ring of stars rotating around a central obscure body, perhaps part of a system of rings rotating around another body, and so on. Even Immanuel Kant, in the same years, proposed an inhomogeneous model: a distribution radially decreasing of worlds, to be identified with galaxies. The wave of evolution goes from inside to outside: while the worlds near the center are already in an advanced stage of evolution, and will perish first, those near the outer boundary are still in the primordial Chaos.

In 1820, Heinrich Olbers presents the famous Olbers' paradox, already formulated by Halley in 1721. Any homogeneous, static and infinite model should be in equilibrium everywhere at the temperature of the star's surfaces. Since this is clearly not so (for instance, the night sky is dark), either the universe is not homogeneous, or is not static (or the light has different properties than those we experiment on Earth, for instance its flux decreases faster than the distance squared). Carl Charlier, in 1908, proposed to abandon the first assumption, the homogeneity, and built a hierarchical model with the stars arranged in such a way that their density seen from any star decreases with distance. Since in Charlier's model the density decreases radially from every star (and not only, as in Kant's model, from the center of the universe), this is in fact the first fractal model of the universe.

The first and, I must add, the last for sixty years. In fact, the powerful action of Einstein's equations, solved in a cosmological setting by Einbstein himself and by Friedmann, de Sitter and Lemaitre, along with the discoveries of Edwin Hubble in the 20's , gave to the Cosmological Principle the status of almost a dogma among cosmologists. According to this, the universe is homogeneous and isotropic when averaged over some scale. This scale of

homogeneity has evolved in time, from a few megaparsecs initially to a few tens of megaparsecs today. It is almost superfluous to add that the cosmological models based on the Cosmological Principle, that is, based on Friedmann's equations, had tremendous successes in explaining the observed facts and in anticipating new discoveries. Two successes rise above all: the prediction of the cosmic microwave background by Gamow, Alpher and Hermann, and the explanation of the cosmic abundance of light elements.

What is not superfluous to add is that the precise quantification of the homogeneity scale lacked (and still lacks, in my opinion) for many years. Maybe the first astronomer to object to the view of a universe homogeneous down to "small" scales of a few megaparsecs has been Gerard de Vaucouleurs, when he realized in the 50's that many galaxies lie on a sort of superplane more than 30 Mpc/h by radius (see e.g. de Vaucouleurs 1970). However, the few and sparse redshifts then available did not allow him to back this view with clear evidences. Only when the redshift campaigns of the 80's were completed (Perseus-Pisces, CfA1), the strong inhomogeneity of our universe became clear, and the scale at which Friedmann's equation are supposed to hold was pushed to something like 30 Mpc/h or more.

In the mean time, the fractals of Benoit Mandelbrot entered the scene. Collecting many disparate ideas on the mathematics of non-differentiable manifolds and of chaotic processes, Mandelbrot (1982) realized that a common structure underlies these concepts. The fractals were introduced as a mathematical tool to investigate the properties of a vast class of phenomena, from turbulence to crystal growth, that are characterized by chaotic behavior. The general property is that in all these phenomena some quantity varies as a power-law on a wide range of the independent variable, whatever this may be. For instance, the number of earthquakes as a function of their intensity, or the number of Moon craters versus their size, decreases as a power law. For the fractal in space, this quantity is simply the number of particles within a distance r from another particle.

Mandelbrot proposed in the 70's that even the distribution of galaxies may follow a fractal law, that is a density scaling with distance. Mandelbrot was inspired by the power-law decrease of the correlation function with distance, proposed in particular by Peebles. The idea was discussed at length in the classic Peebles (1980) textbook, and finally rejected on the ground that the small *amplitude* of the angular correlation function proved large scale homogeneity. This argument, however, appears now to be inconclusive, since the reconstruction of the 3-dimensional structure from the projected one requires the knowledge of the galaxy luminosity function, which, on the other hand, is estimated from catalogs assuming homogeneity. Moreover, many other factors enter the reconstruction, like the galaxy evolution and the relativistic effects. The simultaneous fit of the luminosity function and of the galaxy clustering may well give acceptable results also for the fractal model. Finally, any fractal model has intrinsically a very large variance, so that it is very difficult to rule out it on the basis of correlation amplitude alone. Rather, the full shape of the correlation function is needed.

In the 80's the emphasis shifted to redshift surveys and to the comparison with detailed and physically motivated models of structure formation. The fractal hypothesis was revived by Pietronero and coworkers (Coleman &

Pietronero 1992; Sylos-Labini, Montuori & Pietronero 1998) basing on the new surveys like CfA1 and Perseus-Pisces, who showed the clear trace of density scaling and of strong inhomogeneities. However, in the same years, it appeared clear that even the standard scenario of structure formation, that is the inflationary primordial spectrum with CDM normalized to the microwave background fluctuations, required a density scaling approximately power-law up to, say, 20 or 30 Mpc/h. At the beginning of the 90's, then, the fractal hypothesis and the standard scenarios agreed on fractality up to a few tens of megaparsecs. The question then became: what's beyond? That is, do the redshift data prove homogeneity beyond this scale, or is this only a lower limit? And also, can we infer from other data, like radio and X backgrounds, or cosmic background, what the homogeneity scale is? While the advocates of the fractal hypothesis consider the 30 Mpc/h a lower limit, and point to the many assumptions often made in "proving" homogeneity beyond this, the supporters of the standard model believe that this is really the frontier of the inhomogeneous world, any residual trend being attributed to luminosity bias or relativistic effects. Beyond this distance, modulo a factor not greater than 2, Friedmann's equations are finally on safe ground.

In these lectures I try to present a balanced, albeit personal, view of the issue. Although I see signs of convergence on a common ground, the history of the confrontation between homogeneous and fractal universe, or between small-scale and large-scale homogeneity, will continue for quite a long time.

3.1.3 Notation

ρ_0 average number density
n number density
N number of particles
N_i counts in finite cells
n_i count in a infinitesimal cell, equal to 0 or 1
δ density contrast
s subscript denoting a quantity evaluated in a sample (e.g., R_s, sample size; ξ_s, sample correlation)
c subscript denoting a conditional quantity
V volume
ρ mass density
M_p p-th central moment

In general, I write the dependence on the three spatial coordinates simply as $f(x)$. When the functions are integrated in dV or d^3x I mean the integrand depends on all three coordinates. When the integration is written as r^2dr, I mean that the integrand depends only on the modulus r. A similar convention applies to the wavevector k.

3.2 Estimators

The general problem we want to deal with in this section is to characterize a random distribution of points in space. The main goal is to find a small

number of estimators, able to express the properties of the distributions in a compact way, and which can be efficiently compared to the theory.

3.2.1 Moments of the counts-in-cells

Among infinite possible ways to characterize a distributions of particles, the n-point correlation functions, or their integral average, the moments, are often selected because of their straightforward definition, and because of their easy numerical computation. It is often necessary to think of a distribution of particles as a *finite* and *discrete* sample drawn from an underlying field. We need then to distinguish between the properties of the underlying field, that we sometimes refer to as the "universe", and the properties of the sample under investigation: the sample gives only an estimate of the universe. If we want to infer the properties of the universe from those of the sample, we need to take into account both the finiteness and the discreteness. In particular, we need to assume a model for the behavior of the field *beyond* the sample, and "*beneath*" the particles that sample the field. Two typical assumptions are that the field outside the sample looks like the field inside (fair sample hypothesis), and that the particles are a Poisson sampling of the continuous field (Poisson sampling hypothesis). Both assumptions can be tested only when is possible to obtain a larger and denser sample. Lacking this possibility, which is often the case in cosmology, the assumptions need to be treated with great caution.

Let us begin with the moments. Suppose we partition a distribution of particles into m cells, for instance spherical cells of radius r, *randomly located*, and count the number of particles inside each cell. This gives the counts N_i, with $i = 1, .., m$. Then we can form the number density contrasts

$$\delta_i = (N_i - N_0)/N_0 \tag{5.1}$$

where N_0 is the average count

$$N_0 = \sum N_i/m \tag{5.2}$$

and we can form the p-th order central moment

$$M_p = \langle \delta_i{}^p \rangle = m^{-1} \sum_i \delta_i{}^p \tag{5.3}$$

By definition, $M_0 = 1, M_1 = 0$. Suppose now that the probability to have a density contrast between δ and $\delta + d\delta$ is $P(\delta)d\delta$, where $P(\delta)$ is the probability density function (PDF) of the counts. The moments M_p of the particle distribution are an *estimate* of the moments of the PDF. For instance, the second order moment, M_2 is an estimate of the variance of the number density contrasts. The third order moment is called skewness, while the combination

$$K \equiv M_4 - 3M_2^2 \tag{5.4}$$

is the kurtosis. If the PDF is a gaussian

$$P(\delta) = (2\pi\sigma^2)^{-1/2} \exp\left(-\frac{\delta^2}{2\sigma^2}\right) \tag{5.5}$$

then all its moments depend on σ and both the skewness and the kurtosis vanish. These moments are therefore the simplest estimator of deviation from gaussianity.

In practice we estimate the moments from a finite distribution of particles, i.e. a discrete random sampling of a continuous underlying field, for instance the dark matter field. The number of particles at any given point is then a function of the continuous field. In cosmology, this function is established by the physical processes that led to the formation of the discrete particles, the galaxies, and can be in general extremely complicated. As already mentioned, the simplest assumption we can make is that the galaxies are a Poisson sampling of the mass field, that is, the galaxies trace the mass. In this case, the average density of galaxies in any given region is proportional to the average density of the underlying field. A slightly more complicated assumption can be that galaxies are a Poisson sampling not everywhere, but only when the underlying field is above a certain threshold. This is what is often referred to as biased formation . It is clear that the true physical process can be much more complicated than this, for instance the threshold may vary in space, or the sampling function can be non-local, etc.. In most of what we will say here, the simplest Poisson assumption is always understood.

Assuming Poisson sampling, we immediately encounter the problem of Poisson noise. That is, the number of particles N at a point in which the field is ν, is a random variable distributed as a Poisson variable with mean proportional to ν, say equal to $\eta = \beta\nu$, that is

$$P(N;\eta) = \frac{e^{-\eta}\eta^N}{N!} \tag{5.6}$$

If the field ν is distributed as $f(\nu)$, then the PDF of N is

$$P(N) = \int f(\nu)P(N;\nu)d\nu$$

The moments of N are then a function of the moments of $f(\nu)$ and of $P(N;\nu)$. If we are interested in the properties of the underlying field, we need to estimate the moments of ν, and of the density contrast $\delta\nu/\nu_0$, from the moments of N. This can be done easily exploiting the properties of the generating functions, defined as

$$G(\phi) = \langle e^{\phi x}\rangle = \int e^{\phi x}P(x)dx = \sum_p^\infty \frac{M_p}{p!}\phi^p$$

The moments can then be derived from the generating function (d_p denotes the $p-$th derivative) as

$$M_p = d_p G(\phi)|_{\phi=0}$$

The generating function is particularly useful because in the case of a Gaussian distribution is simply $G(\phi) = \exp(m\phi + \sigma^2\phi^2/2)$ and because one can automatically take into account the moments of the Poisson noise by the substitution $\phi \to e^{\phi} - 1$. For instance, we have that the moments of the density contrast of the continuous field (labelled with an asterisk) in terms of the moments of the discrete realization of N_0 particles is

$$M_2^* = M_2 - N_0^{-1} \tag{5.7}$$

where the second term is the Poisson noise. Moreover, one can define the *cumulants* by the relation

$$K_p = d_p \log G(\phi)|_{\phi=0}$$

The cumulants with $p > 2$ vanish for a Gaussian distribution; the third order cumulant is the skewness and the fourth order is the kurtosis, defined above.

In conclusion, a simple way to describe a distribution of particles is to estimate the lowest moments in cells of varying radius, that is to evaluate $M_2(r), M_3(r), K(r)$ and so on. However, no finite amount of moments do characterize completely the distribution, unless of course we know already that the distribution depends on a finite amount of parameters, e.g. is Gaussian or Poisson, etc.

3.2.2 Conditional density

So far we considered randomly centered cells. However, it is often useful to consider instead cells centered around a particle. The counts inside cells centered on particles have statistical properties different from the counts in random cells. The cells centered on particles are in fact conditioned upon the presence of a particle inside the cell itself. Their moments are therefore *conditional* moments.

Let us consider the first order moment, i.e. the average count or the average density in a sample containing N particles in a volume V. If the cells are random, then clearly the average density inside the cells of any size equals the average density of the whole sample

$$\langle \rho \rangle = N/V = \rho_0 \tag{5.8}$$

But if the cells are centered on particles, then the conditional density inside the cells is in general different from the sample density

$$\langle \rho_c \rangle \neq \rho_0 \tag{5.9}$$

because the number of particles in a cell depends also on the presence of the center particle, unless the particles are uncorrelated. Likewise, all the higher order moments of the conditional density differ from the moments of the random cells, as we will see in the next sections. Of course, when the cell in which $\langle \rho_c \rangle$ is estimated is as large as the sample itself, then $\langle \rho_c \rangle = \rho_0$.

The reason why it is necessary to introduce the conditional density is that we observe the space around us from a particle, i.e. from our galaxy. Therefore, the density we measure in a finite sample around us is a conditional density.

3.2.3 Correlation functions

Other common statistical descriptors are the $n-$point correlation functions. Let $\rho_0 dV$ be the average number of particles in an infinitesimal volume dV , being ρ_0 the average number density. If $dN_{ab} = \langle n_a n_b \rangle$ is the average number of *pairs* in the volumes dV_a and dV_b(i.e., the product of the number of particles in one volume with the number in the other volume), separated by r_{ab}, then the 2-point correlation function $\xi(r_{ab})$ is defined as

$$dN_{ab} = \langle n_a n_b \rangle = \rho_0^2 dV_a dV_b (1 + \xi(r_{ab})) \tag{5.10}$$

If the distribution is Poissonian, then the average number of pairs is exactly equal to the product of the average number of particles in the two volumes, and the correlation ξ vanishes; if there is correlation among the volumes, on the other hand, then the correlation is different from zero. The correlation function is also defined, equivalently, as the spatial average of the product of the density contrast $\delta(r_a) = dN_a/(\rho_0 dV) - 1$ at two different points

$$\xi(r_{ab}) = \frac{dN_{ab}}{\rho_0^2 dV_a dV_b} - 1 = \langle \delta(r_a)\delta(r_b) \rangle \tag{5.11}$$

In practice it is easier to derive the correlation function as the average density of particles at a distance r from another particle. This is a *conditional* density, that is the density of particles at distance r given that there is a particle at $r = 0$. The number of pairs is then the number of particles in both volumes divided by the number of particles $dN_a = n dV_a$ in the volume dV_a at $r = 0$:

$$dN_b = dN_{ab}/dN_a = \rho_0^2 dV_a dV_b (1 + \xi(r_{ab}))/dN_a = \rho_0 dV_b (1 + \xi(r_b)) \tag{5.12}$$

The correlation function can then be defined as

$$\xi(r) = \frac{dN_c(r)}{\rho_0 dV} - 1 = \frac{\langle \rho_c \rangle}{\rho_0} - 1 \tag{5.13}$$

i.e. as the average number of particles at distance r from any given particle (or number of neighbors), divided by the expected number of particles at the same distance in a uniform distribution, minus 1, or *conditional density contrast*. If the correlation is positive, there are then more particles than in a uniform distribution: the distribution is then said to be positively clustered. This definition is purely radial, and does not distinguish between isotropic and anisotropic distributions. One could generalize this definition by introducing the anisotropic correlation function as the number of pairs in volumes at distance r and a given longitude and latitude. This is useful whenever there is some reason to suspect that the distribution is indeed anisotropic, as when there is a significant distortion along the line-of-sight due to the redshift.

If the average density of particles is estimated from the sample itself, i.e. $\rho_0 = N/V$, it is clear that the integral of $dN_c(r)$ must converge to the number of particles in the sample :

$$\int_0^R dN_c(r) = \int \rho(r) dV = N \tag{5.14}$$

In this case the correlation function is a sample quantity, and it is subject to the integral constraint (Peebles 1980)

$$\int_0^R \xi_s(r) dV = N/\rho_0 - V = 0 \tag{5.15}$$

Assuming spatial isotropy this is

$$4\pi \int_0^R \xi_s(r) r^2 dr = 0 \tag{5.16}$$

If the sample density is different from the true density of the whole distribution, we must expect that the $\xi_s(r)$ estimated in the sample differs from the true correlation function. From Eq. (5.13), we see that $g(r) = 1 + \xi(r)$ scales as ρ_0^{-1}. Only if we can identify the sample density ρ_0 with the true density the estimate of $\xi(r)$ is correct. In general, the density is estimated in a survey centered on ourselves, so that what we obtain is in reality a conditional density.

The conditional density at distance r from a particle, averaged over the particles in the survey, is often denoted in the statistical literature as $\Gamma(r)$; we have therefore from Eq. (5.13)

$$\Gamma(r) \equiv \langle \rho_c \rangle = \rho_0 (1 + \xi) \tag{5.17}$$

The average in spherical cells of radius R and volume V of this quantity is denoted as

$$\Gamma^*(R) \equiv \langle \rho_c \rangle_{sph} = \rho_0 (1 + \widehat{\xi}) \tag{5.18}$$

where

$$\widehat{\xi} = V^{-1} \int \xi dV \tag{5.19}$$

To evaluate $\Gamma^*(R)$ one finds the average of the number of neighbors inside a distance R from any particle contained in the sample.

The correlation function can be generalized to more than two points. The 3-point function is defined as

$$\varsigma(r_a, r_b, r_c) = \langle \delta(r_a) \delta(r_b) \delta(r_c) \rangle \tag{5.20}$$

In terms of the counts in infinitesimal cells we can write

$$\begin{aligned} \varsigma(r_a, r_b, r_c) &= \left\langle \left(\frac{n_a}{\rho_0 dV_a} - 1 \right) \left(\frac{n_b}{\rho_0 dV_b} - 1 \right) \left(\frac{n_c}{\rho_0 dV_c} - 1 \right) \right\rangle \\ &= \frac{\langle n_a n_b n_c \rangle}{\rho_0^3 dV_a dV_b dV_c} - \xi_{ab} - \xi_{bc} - \xi_{ac} - 1 \end{aligned} \tag{5.21}$$

so that we obtain the useful relation

$$\langle n_a n_b n_c \rangle = \rho_0^3 dV_a dV_b dV_c (1 + \xi_{ab} + \xi_{bc} + \xi_{ac} + \varsigma_{abc}) \tag{5.22}$$

3.2.4 Scaling among moments

In some simple and interesting cases, the moments M_p of the counts obey the following relation *for any box size* in a certain range of scales

$$S_p = \frac{M_p}{M_2^{p-1}} = const$$

Theoretical motivations for this *scaling* relation include the BBGKY equations in the strongly non-linear gravitational regime (Peebles 1980) and the second-order perturbative expansion of the gravitational evolution of the fluctuations (Fry 1984; Juszkiewicz , Bouchet & Colombi 1993). Moreover, the scaling relation is expected for a generic random variable, as the counts in cells, that are a linear combination of n independent random variables (the $k-$modes of the linear density field), expanding the PDF in powers of $n^{-1/2}$ (Amendola 1994).

The scaling relation has been observed up to several tens of megaparsecs in many surveys (e.g. Gaztanaga 1994). Since the moments are the volume integrals of the correlation function (see e.g. Eq. (5.54) below) we expect that a similar scaling relation holds for the correlation functions themselves. The n-point correlation function is then a linear combination of products of $(n-1)$ two-points correlation functions. For instance, we can assume that

$$\varsigma_{ijk} = Q[\xi_{ij}\xi_{jk} + \xi_{ij}\xi_{ik} + \xi_{ik}\xi_{jk}] \tag{5.23}$$

where Q is independent of the spatial coordinates. We will often make use of such scaling relations.

3.2.5 The angular correlation function

Because the angular position of the galaxies is so much easier to determine than their distance, the angular correlation function has been often employed in astronomy. Here we write down the relation between the two correlations, that is the Limber equation, in order to show some properties.

Let $w(\theta) = \langle \delta(\theta+\alpha)\delta(\alpha) \rangle_\alpha$ be the angular correlation function, where $\delta(\alpha)$ is the density contrast at the angular position α. Then the Limber equation in the non-relativistic limit is (e.g. Peebles 1980)

$$w(\theta) = 2F^{-2} \int x^4 \phi^2(x) \xi(r) dx du \tag{5.24}$$

where, for small angles,

$$\begin{aligned} F &= \int x^2 \Phi(x) dx \\ r^2 &= u^2 + x^2\theta^2 \end{aligned}$$

and where $\Phi(x)$ is the selection function for the angular catalog, defined in terms of the luminosity function $\phi(M)$ as

$$\Phi(x) = \int_{-\infty}^{M(m_0,x)} \phi(M)dM \tag{5.25}$$

for a catalog magnitude-limited at m_0. When the redshift of the galaxies in the catalog increases, it is necessary to take into account the relativistic effects of the expanding universe, the density and luminosity evolution of the galaxies, the $k-$correction of the magnitude, etc.

For a power-law $\xi = Ar^{-\gamma}$ we get

$$w(\theta) = 2AF^{-2} \int x^4(u^2 + x^2\theta^2)^{-\gamma/2}\phi^2(x)dxdu = B\theta^{1-\gamma} \tag{5.26}$$

where

$$\begin{aligned} B &= 2AF^{-2}H_y \int x^{5-\gamma}\phi^2(x)dx \\ H_y &= \Gamma(1/2)\Gamma((\gamma-1)/2)/\Gamma(\gamma/2) \end{aligned} \tag{5.27}$$

Now, if the selection function is a step function, i.e. equals unity up to some scale R and then vanishes, and A is a constant, we obtain

$$B = 2R^{-6}AH_y \int^R x^{5-\gamma}dx = 2R^{-\gamma}AH_y \int_0^1 y^{5-\gamma}dy \sim R^{-\gamma}$$

that is, the correlation function decreases with the depth R.

3.2.6 Power spectrum

One of the most employed statistical estimator for density fields is the power spectrum. In recent years it has been used to quantify the clustering properties in many galaxy surveys (see e.g. Peacock & Nicholson 1991, Fisher et al. 1993; Baugh & Efstathiou 1994; Feldman, Kaiser & Peacock 1994; Park et al. 1994; Lin et al. 1996). The main reason is that almost all theories of structure formation predict a specific shape of the spectrum, because the plane waves evolve independently in the linear approximation of the gravitational equations.

Let $\delta(x)$ be the density contrast of a density field and

$$\delta_k = \frac{1}{V} \int \delta(x)e^{ikx}dV \tag{5.28}$$

its Fourier transform. The power spectrum is defined as

$$P(k) = V\delta_k\delta_k^* \tag{5.29}$$

Notice that the power spectrum has the dimension of a volume. It follows

$$P(k) = \frac{1}{V} \int \delta(x)\delta(y) e^{ik(x-y)} dV_x dV_y \tag{5.30}$$

Now, putting $r = x - y$, since

$$\xi(r) = \langle \delta(y+r)\delta(y) \rangle = \frac{1}{V} \int \delta(y+r)\delta(y) dV_y \tag{5.31}$$

then,

$$P(k) = \int \xi(r) e^{ikr} dV \tag{5.32}$$

Therefore, the power spectrum is the Fourier transform of the correlation function (Wiener-Khintchin theorem). Finally, assuming spatial isotropy, i.e. that the correlation function depends only on the modulus $|r|$, we obtain

$$P(k) = 4\pi \int \xi(r) \frac{sinkr}{kr} r^2 dr \tag{5.33}$$

These definitions refer to infinite samples and to a continuous field. In reality,we always have a finite sample and a discrete realization of the field, i.e.. a finite number of particles. Therefore, we have to take into account the effects of both finiteness and discreteness.

To investigate the discreteness, we assume as field a collection of N particles of dimensionless masses m_i expressed in units of the average mass m_0 at positions x_i, in a volume V . In the following we will make use of the window function $W(x)$, a function which expresses the way in which the particles are selected. A typical selection procedure is to take all particles within a given region, and no particles elsewhere. In this case, the function will be a constant inside the survey, and zero outside. We will always consider such a kind of window function in the following, and normalize it so that

$$\int W(x) dV = 1 \tag{5.34}$$

With this normalization, $W(x) = 1/V$ inside the survey.

Let us now express the field as a sum of Dirac functions

$$\delta(x) = \frac{\rho(x)}{\rho_0} - 1 = \frac{V}{N} \sum_i m_i w_i \delta_i(x - x_i) - 1 \tag{5.35}$$

where $w_i = VW(x_i)$. The Fourier transform is

$$\delta_k = \frac{1}{V} \int \left(\frac{V}{N} \sum_i m_i w_i \delta_i - 1 \right) e^{ikx} dV = \frac{1}{N} \sum_i m_i w_i e^{ikx_i} - W_k \tag{5.36}$$

where we introduced the $k-$space window function

$$W_k = \int W(x) e^{ikx} dV \tag{5.37}$$

normalized so that $W_0 = 1$. In the limit of $V \to \infty$, the window function becomes a Dirac delta $\delta(k)$. Now, the expected value of the power spectrum is

$$P(k) = V\langle \delta_k^2 \rangle \tag{5.38}$$

that is

$$P(k) = \frac{V}{N^2} \sum_{ij} m_i m_j w_i w_j e^{ik(x_i - x_j)} - V W_k^2 \tag{5.39}$$

We used the relation

$$\langle \frac{1}{N} \sum_i m_i w_i e^{ikx_i} \rangle = \frac{1}{N} \sum_i m_i \int W(x) e^{ikx} dV = W_k \tag{5.40}$$

Finally, if the positions x_i and x_j are uncorrelated, we can pick up only the terms with $i = j$, so that, neglecting the window function, which is important only for $k \to 0$, we obtain the pure noise spectrum

$$P_n(k) = \frac{V}{N^2} \sum_i m_i^2 w_i^2 = V/N \tag{5.41}$$

where the last equality holds only if $m_i = 1$ for all particles. The noise spectrum is negligible only for large densities, $\rho_0 = N/V \to \infty$. Since the galaxy distributions are often sparse, the noise is not always negligible and has to be subtracted from the estimate. In Fig. 2.1 we show the power spectrum of a Poisson distribution, oscillating around the expected value. For the power spectrum applies the same consideration expressed for the moments: the power spectrum does not characterize completely a distribution, unless we know the distribution has some specific property, e.g. is Gaussian, or Poisson, etc. In Fig. 2.2 we show two distributions with the same spectrum (at least in some range) but very different higher order properties.

Eq. (5.39) holds both for the whole universe and for a finite sample. Usually astronomers have a finite sample and wish to get information on the whole universe. Here we find the relation between the two; for simplicity, we work in the continuous limit. Let

$$\xi(x) \equiv \langle \delta(x) \rangle_c = \frac{\langle \rho_c(x) \rangle}{\rho_0} - 1$$

be the correlation function in the whole universe, where ρ_0 is the average density. A subscript s will denote as usual *sample* quantities. In a finite sample the density contrast is subject to two corrections. First, the average density in

a finite sample is the integral of the conditional density (it is conditional, let us remark this point once again, because we observe from a particle) within the sample

$$\begin{aligned}\rho_s &= \int \langle \rho(x)\rangle_c W(x) d^3x = \rho_0 (1 + \int \xi(x) W(x) d^3x) \\ &= \rho_0 [1 + (2\pi)^{-3} \int P(k) W(x) e^{-ikx} d^3x d^3k)] = \rho_0 (1 + \widehat{\xi}) \end{aligned} \tag{5.42}$$

where, as in Eq. (5.19), and assuming radial symmetry

$$\widehat{\xi} = \frac{1}{2\pi^2} \int P(k) W(k) k^2 dk \tag{5.43}$$

It follows that there exists a relation between the universe correlation function and the sample correlation function. In fact, from

$$\xi_s(x) \equiv \langle \delta_s(x)\rangle_c = \frac{\langle \rho(x)\rangle_c}{\rho_s} - 1 = \frac{\langle \rho(x)\rangle_c}{\rho_0 (1 + \widehat{\xi})} - 1 \tag{5.44}$$

we obtain the correlation function in the sample as

$$\xi_s = \frac{\xi - \widehat{\xi}}{1 + \widehat{\xi}} \tag{5.45}$$

On the right-hand-side of this equation there are only universe quantities, that cannot be completely known from within the survey. Eq. (5.45) has the immediate consequence that the sample correlation function is coupled to the sample geometry through $\widehat{\xi}$. In particular, its amplitude depends on $\widehat{\xi}$: then, a variation of $\widehat{\xi}$ with the scale induces a variation of ξ_s.

Further, the conditional density contrast is weighted by a window function $W(x)$

$$P_s(k) = V \int \xi_s(x) W(x) e^{ikx} d^3x = (1+\widehat{\xi})^{-1} V \int (\xi(x) - \widehat{\xi}) W(x) e^{ikx} d^3x \tag{5.46}$$

By the convolution theorem, the Fourier transform of a product of functions is the convolution of the individual Fourier transforms. Therefore we obtain

$$\begin{aligned} P_s(k) &= \frac{V}{(2\pi)^3 (1 + \widehat{\xi})} \left[\int P(k') W(k - k') d^3k' - (2\pi)^3 \widehat{\xi} W(k) \right] \\ &= \frac{V}{(2\pi)^3 (1 + \widehat{\xi})} \int P(k') [W(k - k') - W(k) W(k')] d^3k' \\ &= \frac{V}{(2\pi)^3 (1 + \widehat{\xi})} \int P(k') W^*(k, k') d^3k' \end{aligned} \tag{5.47}$$

where $W^* = W(k-k') - W(k)W(k')$. Notice that, because of the integral constraint on $\xi_s(r)$, Eq. (5.16), we have to verify the following condition on any sample estimate of the power spectrum

$$P_s(0) = 4\pi \int_s \xi_s(r) r^2 dr = 0 \tag{5.48}$$

The expression (5.47) does indeed verify this condition, since $W^*(0,k') \equiv 0$. The spectrum of the sample is therefore not only a convolution of the real spectrum with the window function, as often stated, but includes also other corrections due to the finiteness of the sample and to the use of the conditional density. The kernel $W^*(k',k)$ couples modes at different k. In Fig. 2.3 I show $W^*(k',k)$ for various $k = 2\pi/\lambda$; only for small λ the kernel peaks around k'. For large λ, closer to the sample size, the wavenumber k in the sample spectrum corresponds to a larger wavenumber in the universe spectrum. This introduces a strong distortion of the estimated spectrum. Notice that the expression (5.47) applies to a spectrum calculated by Fourier transforming the density field as a function of distance around each particle; that is, the Fourier transform is purely radial. Often the power spectrum is estimated by Fourier transforming the whole three-dimensional distribution, and then averaging over k-shells. This method gives a kernel which involves $W^2(k-k')$, which implies a different coupling to the sample geometry. In practice, the difference is small, and the effects on the universe spectrum are very closely the same.

Of course, in the limit in which $W(k)$ is a Dirac delta, that is if the sample extends to the whole universe, then $\widehat{\xi} = 0$ and the sample spectrum coincides with the universe spectrum. Otherwise, the spectrum normalization and its shape depend on the sample size. In particular, in the important case in which $\widehat{\xi}$ decreases monotonically,

- the spectrum amplitude is always underestimated in finite samples, unless the size of the sample is big enough to give $\widehat{\xi}(R) = 0$ for all larger scales,
- in the limit of $kR_s \gg 1$, i.e. for $\widehat{\xi} \gg 1$, the spectrum $P_s(k)$ becomes independent of the amplitude ,
- the spectrum has a peak at a scale comparable to the sample depth, because of the condition (5.48).

In Figure 2.4 we show some examples of power spectra in finite samples, compared with the spectrum of the universe field. The underestimation and the peak are evident.

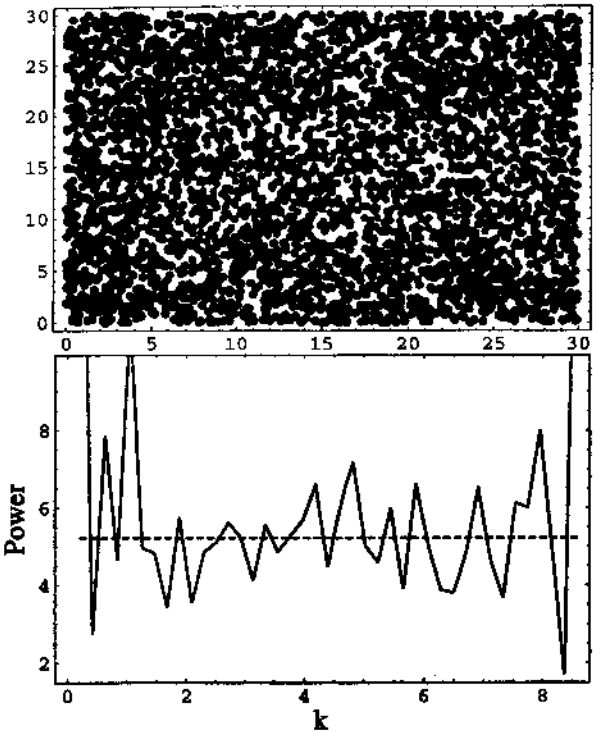

Figure 3.1: Power spectrum of a Poisson distribution. The dashed line is the expected value V/N.

3.2.7 From the power spectrum to the moments

The power spectrum is often the basic outcome of the structure formation theories, and it is convenient to express all the other quantities in terms of it. Here we find the relation between the power spectrum and the moments of the counts in random cells.

Consider a finite cell. Divide it into infinitesimal cells with counts n_i either zero or unity. We have by definition of ξ

$$\langle n_i n_j \rangle = \rho_0^2 dV_i dV_j [1 + \xi_{ij}] \tag{5.49}$$

The count in the cell is $N = \sum n_i$. The variance is then $M_2 = (\langle N^2 \rangle - N_0^2)/N_0^2$ where

$$\begin{aligned} \langle N^2 \rangle &= \langle \sum n_i \sum n_j \rangle = \sum \langle n_i^2 \rangle + \sum \langle n_i n_j \rangle = \\ & N_0 + N_0^2 \int dV_i dV_j W_i W_j [1 + \xi_{ij}] \end{aligned} \tag{5.50}$$

where $N_0 = \rho_0 V$ is the count average, and $\xi_{ij} \equiv \xi(|\mathbf{r}_i - \mathbf{r}_j|)$. Let us simplify the notation by putting

$$W_i dV_i = dV_i^*$$

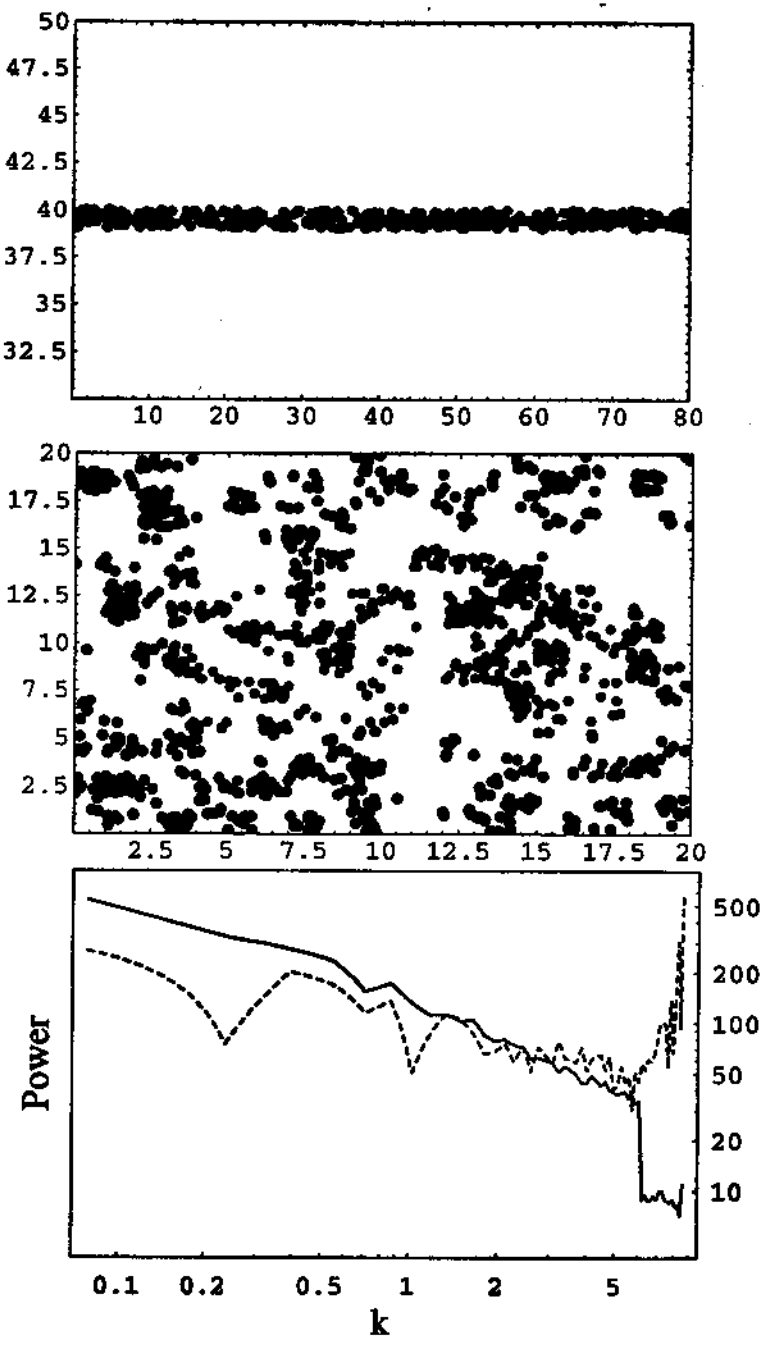

Figure 3.2: Two distributions of particles with similar large scale power spectrum. In the bottom panel, the thin line refer to the top distribution, the dashed line to the distribution in the middle panel.

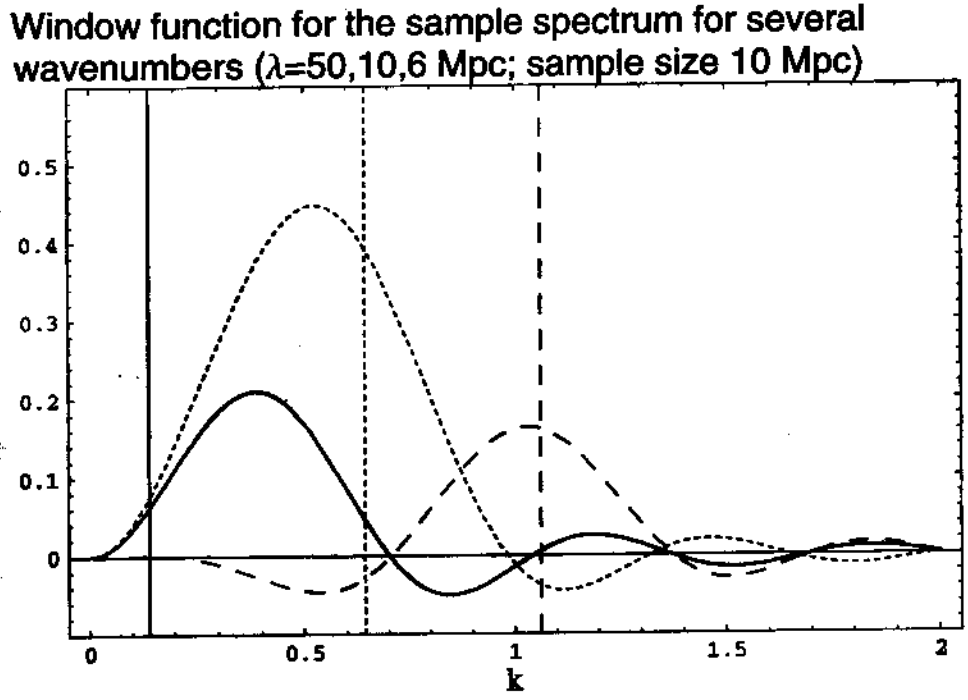

Figure 3.3: The kernel $W^*(k,k')$ **for three values of** $k = 2\pi/\lambda$ **and for a sample size 10 Mpc/**h**. The thin line corresponds to** $\lambda = 50$ **Mpc/**h**; the dotted line to** $\lambda = 10$ **Mpc/**h**; the dashed line to** $\lambda = 6$ **Mpc/**h**. The vertical lines give the location of the three wavelengths. For small** λ **the kernel peaks around** $k' = k$**; for larger** λ**, the kernel peaks at a smaller** λ**, distorting the universe spectrum.**

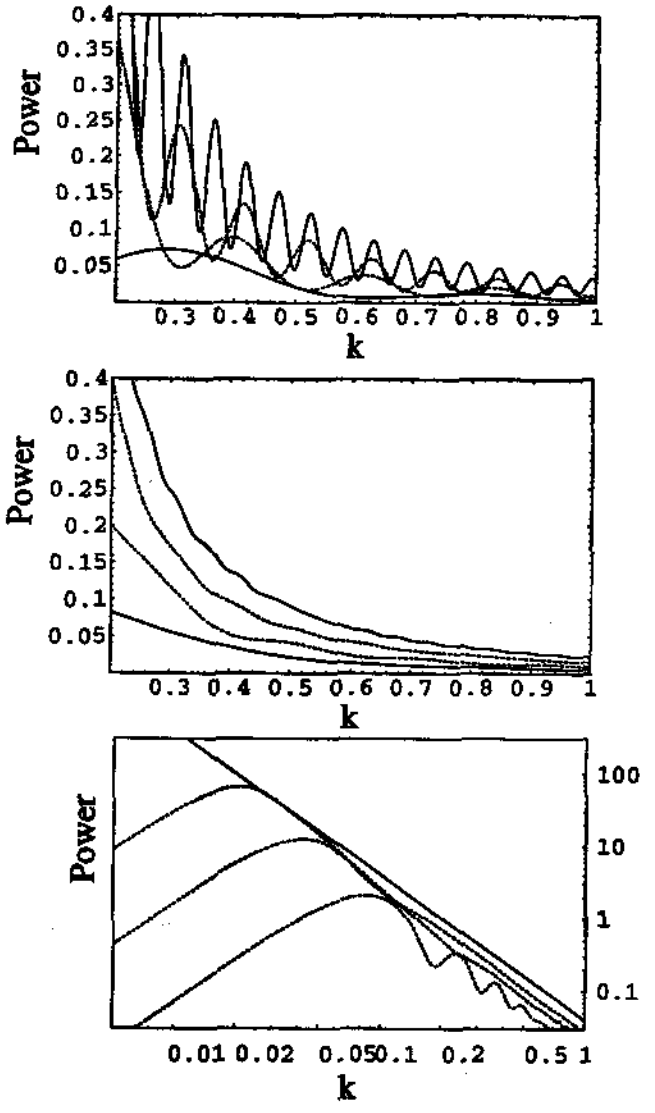

Figure 3.4: Power spectrum estimated in finite samples. The universe spectrum is a power-law spectrum k^{-2} **with arbitrary normalization. In the top panel I show $P_s(k)$ in three samples of 15, 30, 60, 120 Mpc/h at small scales. The riddles are due to the kernel function W^*; in practice, they are averaged out because the spectrum is integrated in $k-$bins. The effect of smearing is shown in the middle panel; here the amplitude increase from the smallest to the largest sample is clear. In the bottom panel the smoothed spectrum estimated in samples of 50, 100 and 200 Mpc/h is compared to the universe spectrum. Both the amplitude increase and the artificial turnover are evident.**

We define the integral (by definition $\int W dV = \int dV^* = 1$ for any window function)

$$\sigma^2 = \int dV_1^* dV_2^* \xi_{12} \tag{5.51}$$

Inserting the power spectrum we have

$$\sigma^2 = (2\pi)^{-3} \int P(k) e^{i\mathbf{k}(\mathbf{r}_1 - \mathbf{r}_2)} W_1 W_2 d^3k d^3r_1 d^3r_2 \tag{5.52}$$

This becomes, for *spherical cells*,

$$\sigma^2 = (2\pi^2)^{-1} \int P(k) W^2(k) k^2 dk \tag{5.53}$$

Finally we obtain the relation between the power spectrum (or the correlation function) and the second-order moment of the counts:

$$M_2 = N_0^{-2} \langle (\Delta N)^2 \rangle = N_0^{-2} (\langle N_i^2 \rangle - N_0^2) = N_0^{-1} + \sigma^2 \tag{5.54}$$

where $\Delta N = N - N_0$. The first term is the noise, the second term is the count variance in the continuous limit.

For the third order moment we proceed in a similar fashion:

$$\begin{aligned} \langle N^3 \rangle &= \langle \sum n_i \sum n_j \sum n_k \rangle = \sum \langle n_i^2 \rangle + \sum \langle n_i^2 \rangle \sum n_i + \sum \langle n_i n_j n_k \rangle \\ & N_0 + 3N_0^2 + N_0^3 \int dV_i^* dV_j^* dV_k^* [1 + \xi_{ij} + \xi_{ik} + \xi_{jk} + \varsigma_{ijk}] \end{aligned} \tag{5.56}$$

where in the last equality we used the definition of the three point correlation given in Eq. (5.22)

$$\langle n_i n_j n_k \rangle = \rho_0^3 dV_i dV_j dV_k [1 + \xi_{ij} + \xi_{ik} + \xi_{jk} + \varsigma_{ijk}] \tag{5.57}$$

The third order moment is then

$$M_3 = N_0^{-3} \langle (\Delta N)^3 \rangle = N_0^{-2} + \int dV_i^* dV_j^* dV_k^* \varsigma_{ijk} \tag{5.58}$$

If we can assume the scaling relation $\varsigma_{ijk} = Q[\xi_{ij}\xi_{jk} + \xi_{ij}\xi_{ik} + \xi_{ik}\xi_{jk}]$ then we can express M_3 in terms of $P(k)$ and of the new parameter Q. In the limit of large N_0, a Gaussian field ($M_3 = 0$) has $Q = 0$.

3.2.8 The variance of the conditional density

In view of the application to fractals, it is important to derive the variance of the conditional density as a function of the power spectrum. Let $N_c = \sum n_i$ be the count in a cell around a particle located in dV_k (we can call it the conditional count) and let

$$\langle N_c \rangle = N_0(1 + \widehat{\xi}) \tag{5.59}$$

be its average, where $\widehat{\xi}$ has been defined in Eq. (5.42) as

$$\widehat{\xi} = \int dV^* \xi(r) = (2\pi)^{-3} \int P(k) W(k) d^3k$$

The correlation between the counts in the infinitesimal cells n_i is

$$\langle n_i n_j \rangle_c = \langle n_i n_j n_k \rangle / \langle n_k \rangle = \rho_0^2 dV_i dV_j [1 + \xi_{ij} + \xi_{ik} + \xi_{jk} + \varsigma_{ijk}] \tag{5.60}$$

from which we have

$$\begin{aligned} \langle N^2 \rangle_c &= \langle \sum n_i \sum n_j \rangle_c = \\ &= N_0(1 + \int dV^* \xi) + N_0^2 \int dV_i^* dV_j^* [1 + \xi_{ij} + \xi_{ik} + \xi_{jk} + \varsigma_{ijk}] \end{aligned} \tag{5.61}$$

The dimensionless conditional density variance, again assuming the scaling relation (5.23), is then

$$\sigma^2_{\rho_c} \equiv \frac{\langle \rho_c^2 \rangle - \langle \rho_c \rangle^2}{\rho_0^2} = \frac{\langle N_c^2 \rangle - \langle N_c \rangle^2}{N_0^2} = N_0^{-1}(1+\widehat{\xi}) + \sigma^2 - \widehat{\xi}^2 + Q(\widehat{\xi}^2 + 2K_2) \tag{5.62}$$

The last term in the expression can be written as (Peebles 1980)

$$K_2 = \int dV_i^* dV_j^* \xi(r_i) \xi(r_{ij}) \tag{5.63}$$

In the important case in which ξ is a power law, it can be shown that a very good approximation is

$$K_2 \simeq \sigma^2 \widehat{\xi} \tag{5.64}$$

For instance, if $\xi \sim r^{-1}$ it turns out that $K_2 = 1.04\sigma^2\widehat{\xi}$. In the following, we will always assume Eq. (5.64).

The first term in Eq. (5.62) is the Poisson noise, which vanishes in the limit of large N. Notice that this expression implies a lower limit on the skewness term Q, because the variance is a positive-definite quantity (see Peebles 1980). When the Poisson noise can be neglected, the limit is

$$Q \geq \frac{\widehat{\xi}^2 - \sigma^2}{\widehat{\xi}^2 + 2\widehat{\xi}\sigma^2} \tag{5.65}$$

This implies that the density field cannot be exactly Gaussian, as already remarked. In the limit of strong correlation, i.e. at small scales, $\widehat{\xi}^2$ dominates over σ^2 because the former is quadratic in the correlation. Then, since $\widehat{\xi}$ is of the same order as σ^2 for reasonable window functions, we obtain $Q \geq 1/3$. Notice also that all this holds only if the 3-point correlation function can be expressed as in Eq. (5.22), a non-trivial condition indeed. However, as already observed, many observations and the modeling of gravitational clustering seem to support such a behavior.

In the opposite limit of small correlation, i.e. at scales larger than the homogeneity scale, σ^2 is the dominating term, and

$$\sigma^2_{\rho_c} = \sigma^2 \tag{5.66}$$

To conclude this Section, consider the definition of $\Gamma^*(R)$ in Eq. (5.18)

$$\Gamma^*(R) \equiv \langle \rho_c \rangle_{sph} \tag{5.67}$$

In practice, $\Gamma^*(R)$ is evaluated calculating the conditional density in cells centered around each particle and averaging. Suppose this is done for m particles. The variance for each cell is as in Eq. (5.62), but the variance of the average $\Gamma^*(R)$ tends to be m times smaller, in the limit in which the cells are independent of each other. In practice, this is never the case, and a Monte Carlo method should be employed. It is clear, however, that the variance of $\Gamma^*(R)$ is expected to be much smaller than that of $\langle \rho_c \rangle$ for the whole sample.

3.3 Predictions

3.3.1 Introduction to CDM-like models

In this Section we use the term CDM-like models to define all the various fluctuation models which share the following properties:

- The fluctuations have Gaussian initial conditions
- They grow only via gravitational instability
- They are normalized to the microwave background fluctuations
- The luminous matter traces the dark matter up to a bias factor of order unity

The prototypical model is characterized by the linear CDM power spectrum

$$P(k) = AkT^2(\Gamma, k) \tag{5.68}$$

where the transfer function $T(\Gamma, k)$, which is somewhat author-dependent, can be approximated by (Bond & Efstathiou 1984)

$$T(\Gamma, k) = \left[1 + (ak + (bk)^{1.5} + (ck)^2)^\nu\right]^{-1/\nu} \tag{5.69}$$

where

$a = (6.4/\Gamma)$ Mpc/h, $b = (3.0/\Gamma)$ Mpc/h, $c = (1.7/\Gamma)$ Mpc/h,

$\nu = 1.13(5.70)$

and $\alpha = \alpha_0 n$ if $\alpha_b \to 0$. This model can be easily generalized to include a tilted primordial slope and a value of Ω_b not negligible:

$$P(k) = Ak^n T^2(\Gamma e^{-\Omega_b - (2h)^{0.5}\Omega_b/\Omega}, k) \tag{5.71}$$

Other generalizations of the CDM paradigm can be embodied in the shape parameters Γ. The spectrum normalization and Γ form the main product of most large scale structure observations.

If we refer to the spectrum of the mass fluctuations, then we normalize either by matching to the microwave background fluctuations or to some other observations like the abundance of clusters or velocity fields. If we want to describe the fluctuations of the luminous matter, be it galaxies, or clusters, or a subclass of either, then we normalize to the observed variance of the class of object at the present time. However, in the latter case, we have to include the redshift correction. In fact, what we measure in redshift surveys is the sum of the line-of-sight recession velocity and the line-of-sight peculiar velocity of the galaxies, rather than their distance. Since the peculiar velocity field depends on the gravitational field, there is a coupling between the matter fluctuations and the redshift of the galaxies. Where the galaxies are virialized, e.g. in the cluster cores, the galaxies in redshift space look less clustered than in real space; where, on the contrary, the galaxies are still in the linear regime, the redshift space clustering is larger than the real space one. As a consequence, in redshift space, there is more power on the large scales and less on the small ones, compared to the real space spectrum. Using the subscript *sp* to label real space quantities, and r to label redshift space ones, we can summarize the two effects by the semi-empirical law (Peacock & Dodds 1994; see also Tadros & Efstathiou 1996):

$$\begin{aligned} P_r(k) &= P_{sp}(k)G(\beta, y) \\ G(\beta, y) &= \frac{\pi^{1/2}}{8}\frac{\mathrm{erf}(y)}{y^5}[3\beta^2 + 4\beta y^2 + 4y^4] - \frac{\exp(-y^2)}{4y^4}[\beta^2(3 + 2y^2) + 4\beta y^2] \end{aligned}$$

where $y = k\sigma_v H_0^{-1}$, σ_v is the cloud velocity dispersion along the line of sight, $\beta = \Omega^{0.6}/b$ and b is the dark matter bias factor, i.e. the ratio of the power spectrum of the galaxies with the spectrum of the total matter field. On small scales, the effect is to change the slope by a factor k^{-1}; on large scales, the effect is to raise the amplitude by the constant

$$f(\beta = \Omega_0^{0.6}/b) = 1 + 2\beta/3 + \beta^2/5 \tag{5.73}$$

When we use this correction, we adopt the value $\sigma_v = 300$ km/sec. We will drop in the following the subscripts r and *sp*, and specify if we are adopting the redshift correction when needed. In Fig. 3.1 the effect of the redshift correction is shown. At small scales, the power spectrum is distorted from

the theoretical predictions also by the non-linear growth of the structures. The CDM linear power spectrum is therefore valid only at scales larger than roughly 10 Mpc/h .

The variance in spherical top-hat cells of radius 8 Mpc/h in terms of the spectrum is, from Eq. (5.53),

$$\sigma_8^2 = (2\pi^2)^{-1} \int P(k) W_8^2(k) k^2 dk \tag{5.74}$$

where $W_8(x = k \cdot 8\mathrm{Mpc}/h) = 3x^{-3}(\sin x - x \cos x)$. Let us consider some class of objects:

- IRAS galaxies: $\sigma_8 \simeq 0.8$ (Fisher 1993);
- CfA2 galaxies $M < -19.7$, $R < 101$ Mpc/h: $\sigma_8 \simeq 1$ (Park et al. 1994);
- CfA2 galaxies $M < -20.3$ $R < 130$: Mpc/h $\sigma_8 \simeq 1.2$ (Park et al. 1994);
- SSRS2, galaxies from $M < -18$ to $M < -21$ and $R < 48$ Mpc/h to $R < 168$Mpc/h: σ_8 increases from 0.6 to 1.7 (Benoist et al. 1996);
- APM clusters ($R < 400$ Mpc/h): $\sigma_8 \simeq 2$ (Gaztanaga, Croft, Dalton 1995);
- Las Campanas galaxies, whole magnitude limited sample, $\sigma_8 \simeq 1$ (Lin et al. 1996).

In Fig. 3.2 the CDM spectrum is compared to the CfA2 data of Park et al. (1996).

For as concerns the total matter, the cluster abundance gives a normalization which depends on Ω_0 (White, Efstathiou, & Frenk 1993)

$$\sigma_8 \simeq 0.5 \Omega_0^{-0.5} \tag{5.75}$$

The COBE normalization is instead given in terms of the constant A which appears in Eq. (5.68). For small ℓ (when the Sachs-Wolfe effect is the dominating one) we have in a flat universe (see. e.g. Padmanabhan 1993)

$$C_l = \frac{A H_0^{n+3} \Omega_0^{1.54}}{16} \frac{\Gamma[3-n]}{\Gamma^2[(4-n)/2]} \frac{\Gamma[(2\ell+n-1)/2]}{\Gamma[(2\ell+5-n)/2]} \tag{5.76}$$

where C_ℓ is the variance of the angular multipole ℓ, $C_\ell = \langle |a_m^\ell|^2 \rangle$. Sometimes the quadrupole $Q_{rms} \equiv (5C_2/4\pi)^{1/2} T_0$ is used to normalize the spectrum, $T_0 \simeq 2.735$K being the radiation temperature. Most experiments produce likelihood contours for Q_{rms} and n. Assuming $n = 1$, values like $Q_{rms} \simeq 15 - 20 \mu K$ are often quoted (e.g. Bennett et al. 1996). For a CDM spectrum, this gives roughly (Efstathiou, Bond, & White 1992)

$$\sigma_8 \simeq 2\Omega_0 h$$

Finally, the velocity field normalization, obtained from IRAS galaxies in a sample 60 Mpc/h deep gives (Zaroubi et al. 1997)

$$\sigma_8 \simeq 0.9\Omega_0^{-0.6}$$

Although the CDM-like models contain fluctuations on all scales, and thus are not, strictly speaking, homogeneous models, the amount of power on large scales is very small. As we will see below, the most common CDM-like models predict a rapid approach to effective homogeneity (that is, to a distribution indistinguishable form the homogeneous one) on scales around 50 Mpc/h. It is important to realize, however, that the homogeneity scale depends on the details of the spectrum, and in particular on its normalization. The clusters, for instance, which are the objects with the highest variance, are more inhomogeneous than the IRAS galaxies, or the total matter normalized to the abundance of clusters.

One of the problem one encounters in discussing CDM models with respect to fractals, is that the normalization of the CDM spectrum depends on the class of objects, as we have seen. The possibility that this dependence is systematic cannot be discarded. For instance, many observations seem to require a strong increase of the spectrum amplitude with the luminosity of the galaxy, or on the richness class of the clusters (e.g. Benoist et al. 1996). Since usually deeper surveys select on average intrinsically brighter galaxies, the dependence on luminosity becomes an apparent dependence on sample size, to the effect that larger samples give higher spectrum normalization, and consequently a larger homogeneity scale. As we will see below, this trend is qualitatively the same for the fractal model. Therefore, *a fractal mimics a CDM spectrum with luminosity segregation.* Breaking the degeneracy between luminosity and fractality is one of the biggest problem to face.

Another important point to realize, in view of the discussion below, is that the normalization of the power spectrum through observations in finite samples depends in general on the sample size, as we have seen in the Section 2.6. The normalization estimated in finite samples coincides with the true normalization only if the sample is much larger than the homogeneity scale. As we will argue below, it is not yet proved that the samples that have been used in literature are that large. If this is so, the value of σ_8 given above may depend on the sample size.

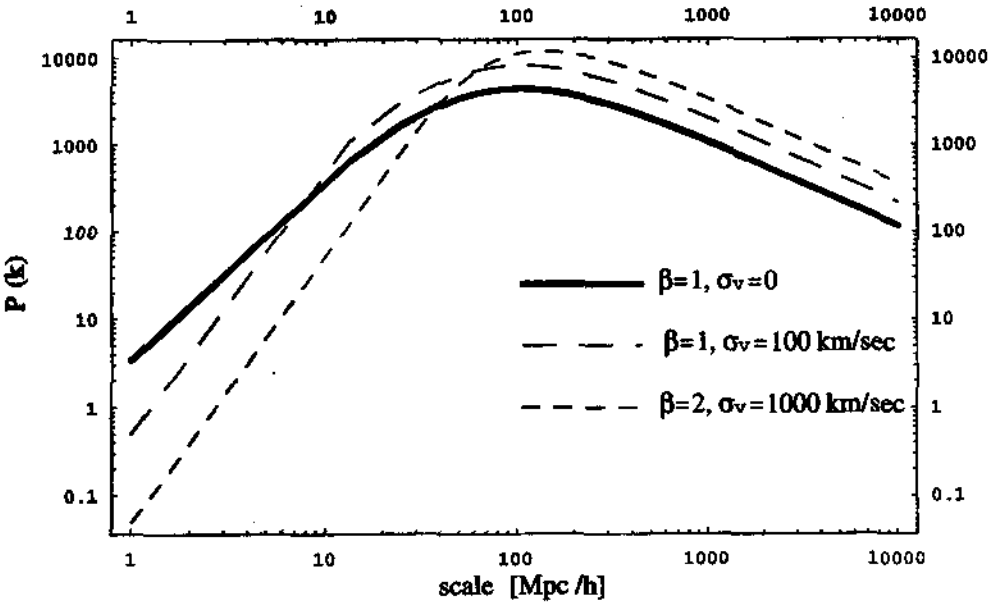

Figure 3.5: Effect of the redshift correction. At small scales, the slope is increased by a factor
k; **at large scales, the amplitude is enhanced by a constant factor. The thick line is a CDM spectrum in real space; the short-dashed line includes redshift correction with $\beta = 2$ and $\sigma_v = 1000$ km/sec; the long-dashed line has $\beta = 1$ and $\sigma_v = 100$ km/sec.**

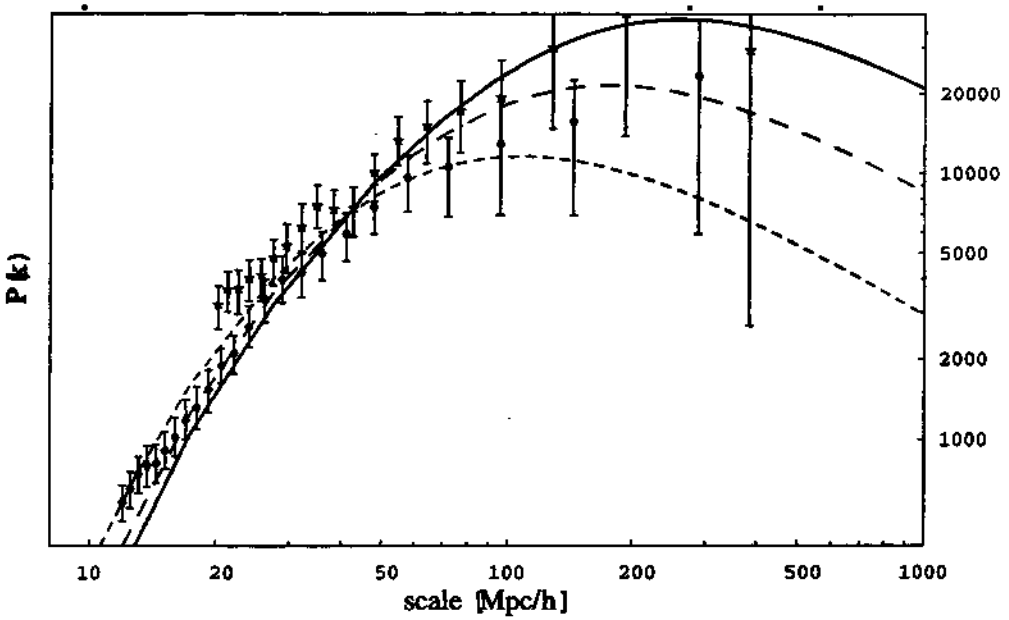

Figure 3.6: The CfA2 data and the CDM spectrum, with redshift correction, and with $\Gamma = 0.2$ **(thin line)**, $\Gamma = 0.3$ **(long dashed line)**, $\Gamma = 0.5$ **(short dashed line), and normalization** $\sigma_8 = 1.2$.

3.3.2 Introduction to fractals

In the current usage, a fractal is any quantity that varies as a power-law. The number of hurricanes or of earthquakes as a function of their energy, or the length of a coastline as a function of the length of the rod employed to measure it, are examples of fractals. In the distribution of galaxies, the fractal quantity is the conditional density (Pietronero 1987; Coleman, Pietronero & Sanders 1988). Suppose we have a large spherical volume of radius R_0 containing N_0 particles. This distribution is a fractal if the *average* number of particles in a sphere of radius $r < R_0$ around a particle scales as

$$\langle N_c(< r)\rangle = Br^D \tag{5.77}$$

where D is the fractal dimension and B is a constant which depends on the sample density. In the following I sometimes omit the brackets $\langle\rangle$ to simplify the notation, but always refer to the average conditional density, unless otherwise stated. If our universe contains $N_0 = 4\pi\rho_0 R_0^3/3$ particles, ρ_0 being the density, then $N_c(< R_0) = N_0 = BR_0^D$, from which

$$B = \frac{4\pi}{3}\rho_0 R_0^{3-D}$$

The average density inside a spherical sample of radius R_s embedded in a larger box of size R_0 is clearly

$$\rho_c = \rho_0 (R_s/R_0)^{D-3} \tag{5.78}$$

In other words, each particle sees around itself a density which decreases as R_s^{D-3}. Notice that this is the average behavior; some particles can see the density increase locally, or experiment different dimensions. Also, notice that this is a *conditional* density: is the density *around particles*, that is, the density in a sphere provided that there is a particle at the center.

As an extremely simple example of a fractal, consider particles distributed on a thin plane with surface density ρ_{sd}. Each particle sees around itself, in a sphere of radius r, N_c particles,

$$N_c(< r) = \pi\rho_{sd} r^2 \tag{5.79}$$

This is therefore a fractal with dimension $D = 2$, as expected since the plane is 2-dimensional. If the plane is in a spherical box of radius R_0, the density of particles inside a radius r is $\rho_0 (R_s/R_0)^{-1}$ where $\rho_0 = 3\rho_{sd} R_0^{-1}/4$, as in Eq. (5.78). A similar case is shown in Fig. 3.3: the spectrum of a $D = 1$ fractal in a plane. This planar distribution is a convenient image of a simple fractal, and can be used to help the intuition. Naturally, is a completely deterministic fractal, and certainly not a realistic description of the galaxy distribution. However, a preference for a planar distribution can be seen for many galaxies, for instance around large voids, and this can explain why $D = 2$ is indeed the observed dimension, at least up some scale.

From Eq. (5.78) we can derive the operative definition of fractal dimension of a distribution of particle as

$$D = 3 + \frac{d\log \rho_c}{d\log r} = \frac{d\log N_c}{d\log r} \tag{5.80}$$

For a homogeneous distribution, $D = 3$, and $\rho_c = \rho_0$. In all other cases, $\rho_c > \rho_0$. Strictly speaking, D is a constant independent of r. However, for real distributions this is never the case, because there are at least a lower and an upper cutoff to fractality. Here we will not adhere to the pure mathematical point of view, and will consider as fractal behavior any trend of N_c for which $D(R_s)$ is not equal to the homogeneous limit 3. The mathematical fractal with $D = const$ is therefore only a limiting case.

There are two important points which are of fundamental relevance to what we will say in the following:

- Every estimate of the density we make in real observations are estimate of the conditional density, because we observe from a "particle"
- The conditional density *systematically* decreases for larger and larger samples, as it goes like R_s^{D-3}

As a consequence of both remarks, the error one makes in identifying the conditional density ρ_c with the universe density ρ_0 is systematic, as opposed to random, and modifies all our statistics, as we will see in the next sections. For instance, the number density contrast we derive in a fractal differs from the true density contrast, and increases with the sample size:

$$\frac{\rho(x)}{\rho_c} \sim \frac{\rho(x)}{\rho_0}(R_s/R_0)^{3-D} \tag{5.81}$$

All quantities based on the density contrast will scale in a similar way. As it can be seen, Eq.(5.78) or (5.81) are a particular case of Eq. (5.42). That is, the fractal distribution is just a particular case of a inhomogeneous distribution.

The correlation function of a fractal is readily evaluated. Consider a sample of radius R_s. As we have seen, the density of particles in the sample is the average conditional density in the spherical cell of radius R_s, $\rho_c = \rho_0(R_s/R_0)^{D-3}$.The scale R_0 at which we define ρ_0 is of no importance here and will drop out in the following. The conditional density in a shell at distance r from a particle is

$$\rho_s = \frac{dN_c(<r)}{4\pi r^2 dr} \tag{5.82}$$

The sample correlation function is the conditional density contrast, i.e. (Coleman & Pietronero 1992)

$$\xi_s(r) = \frac{\rho_s}{\rho_c} - 1 = \frac{D}{3}\left(\frac{r}{R_s}\right)^{D-3} - 1 \tag{5.83}$$

Let us notice some important properties of this expression:

- The correlation amplitude increases with the sample size R_s
- The function $g(r) = 1 + \xi(r)$,rather than $\xi(r)$, is a pure power-law
- The slope of $g(r)$ gives the fractal dimension of the distribution minus 3 (or codimension)
- The correlation function equals unity at

$$r_0 = R_s(D/6)^{1/(3-D)} \tag{5.84}$$

- The correlation function crosses zero at $r_c = R_s(D/3)^{1/(3-D)}$

From the fractal correlation we can immediately derive the quantities σ and $\widehat{\xi}$ introduced in Eq. (5.51) and Eq. (5.42). For a sphere of size r they are

$$\widehat{\xi} = \int \xi(r) dV^* = (R_s/r)^\gamma - 1 \tag{5.85}$$

$$\sigma^2 = \int \xi(r_{12}) dV_1^* dV_2^* = \frac{D}{3}\left(\frac{R_s}{r}\right)^\gamma J_2(\gamma) - 1 \tag{5.86}$$

where $\gamma = 3 - D$ and (Peebles 1980)

$$J_2(\gamma) = 72/\left[(3-\gamma)(4-\gamma)(6-\gamma)2^\gamma\right]$$

In the limit of large R_s, which should always be understood when we refer to theoretical fractals, we have simply $\widehat{\xi} \sim \sigma^2 \sim r^{D-3}$.

We end this section commenting on the definition of fractal dimension given in the literature. There are different definitions of fractal dimension, which depend on exactly which power-law quantity is investigated. The dimension we defined is usually called the correlation dimension D_2, and other definitions, like the Hausdorff dimension or the box-counting dimension can be given. These dimension are completely equivalent in all practical cases. Also, it is to be noticed that the dimension is usually defined in the limit of $r \to 0$, i.e. for boxes vanishingly small. However, galaxy distribution being a distribution of discrete particles, this limit cannot be taken, and the fractal dimension will, in general, depend on the size r of the boxes. The fractal dimension, however, cannot characterize completely a distribution of points, just as it is not characterized completely by the two-point correlation function or the power spectrum.

In the fractal literature, in place of the higher-order moments, the spectrum of dimensions has been introduced (see. e.g. Paladin & Vulpiani 1987). Let N_i be the number of particles within distance r in the cell around the i-th particle, and $\langle N \rangle_c$ its average. Then we define the Minkowski-Bouligand dimensions as (neglecting again the limit for small r) the average of the power of conditional counts

$$D_q = \frac{1}{q-1}\frac{d\log N_c^{q-1}}{d\log r} \tag{5.87}$$

If the dimensions D_q are different, the distribution is called a *multifractal*. The correlation dimension (5.80) is then D_2; the dimension D_3 is in effect

$$D_3 = \frac{1}{2}\frac{d\log\langle N_c^2\rangle}{d\log r}$$

where $\langle N_c^2\rangle$ is given in Eq. (5.62) (neglecting the Poisson term) as

$$\langle N_c^2\rangle = \langle N_c\rangle^2 + N_0^2\left[\sigma^2 - \widehat{\xi}^2 + Q(\widehat{\xi}^2 + 2\widehat{\xi}\sigma^2)\right]$$

It follows, for $R_s \ll R_t$, and if Q does not depend on r

$$D_3 = D_2$$

In a similar way, it can be easily shown that $D_q = D_2$ if the scaling relations among the moments hold. A distribution with all identical dimensions is called a *monofractal*. Therefore, the hierarchical scaling implies monofractality (see e.g. Balian & Schaeffer 1988; Borgani 1995), at least for order $q > 1$.

3.3.3 The power spectrum in fractal models

The power spectrum of a fractal within a spherical sample can be easily derived from Eq. (5.83) :

$$\begin{aligned} P_s(k) &= \int \xi_s(r)W(r)e^{i\mathbf{k}\mathbf{r}}d^3\mathbf{r} = 4\pi\int \xi_s(r)W(r)\frac{\sin kr}{kr}r^2dr \\ &= \frac{4\pi}{3}\left[2+\cos(kR_s)\right]R_s^{3-D}k^{-D} - 4\pi\sin(kR_s)k^{-3} \end{aligned} \qquad (5.88)$$

where the second line applies only if $D \simeq 2$ and the window is a top-hat sphere. The general trend, as can be seen in Fig. 3.4, is that the fractal spectrum rises at small scales as $(8\pi/3)R_s^{3-D}k^{-D}$, reaches a peak at a scale comparable with the sample size, $k_p = 2\pi/(1.5R_s)$, and then turns down as k^2. It is interesting to remark that a qualitatively similar behavior is predicted, for totally different reasons, in the most popular theories of structure formation. Also notice that, as for the correlation, the power spectrum scales with the sample size, increasing linearly if $D = 2$.

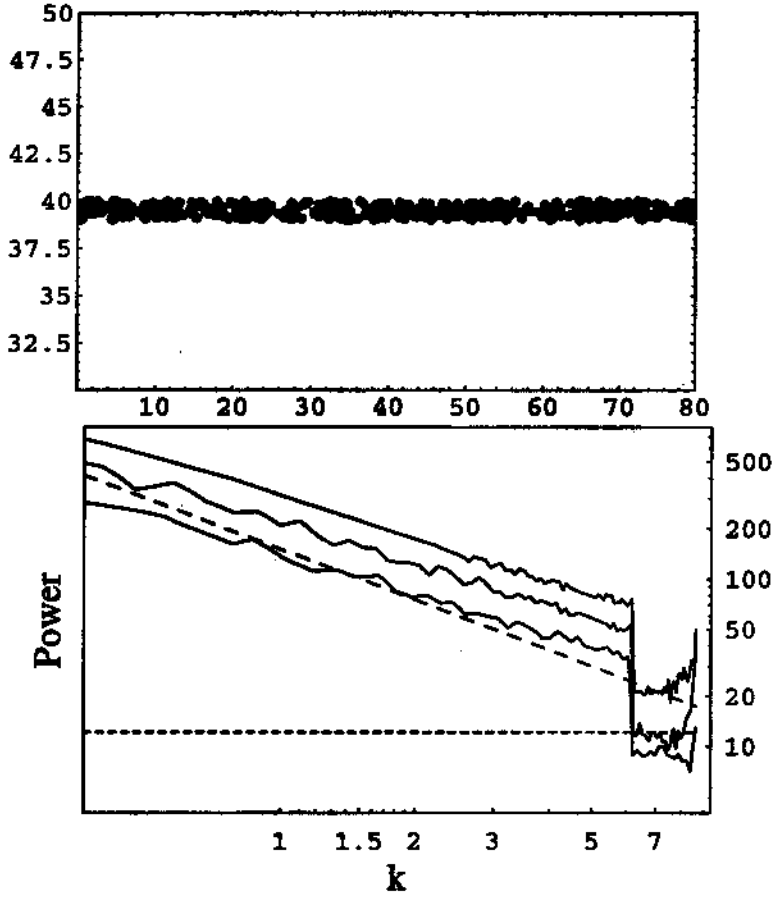

Figure 3.7: Top: linear distribution of particle, a particular case of a $D = 1$ **fractal. Bottom: power spectrum of the distribution in samples of increasing size (from bottom to top). At large k the power comes from the random distribution inside the thickness of the stripe.**

3.3.4 How can we test fractals?

Since the average conditional density estimated in a sample is so important in the statistical measures of a fractal, we need now to derive its variance. The variance of the conditional density is, by Eq. (5.62) and neglecting the Poisson noise

$$\sigma^2_{\rho_c} = \langle \rho_c^2 \rangle - \langle \rho_c \rangle^2 = \rho_0^2 \left[\sigma^2 - \widehat{\xi}^2 + Q(\widehat{\xi}^2 + 2\sigma^2 \widehat{\xi}) \right]$$

Neglecting σ^2 and $\widehat{\xi}$ with respect to $\widehat{\xi}^2$, i.e. in the limit of $R_s \gg r$, we obtain from Eqs. (5.86)

$$\Sigma \equiv \frac{\sigma_c^2}{\langle \rho_c \rangle^2} \simeq Q \left(1 + \frac{2DJ_2(\gamma)}{3} \right) - 1 \tag{5.89}$$

For instance, for $Q = 1$ and $D = 2$, as some observations suggest, $\Sigma = 8/5$. Therefore, the variance of the conditional density can be of the same order of the conditional density itself. In Fig. 3.5 we show the dimensionless variance versus r for some values of Q. In Fig. 3.6 the contour plot of the variance $\Sigma(Q, D)$ in the limit $R_s/r \gg 1$ is displayed. For the interesting values of Q and D the variance is always of order unity. It is however also possible to find special distributions for which the variance vanishes, namely those with $Q = (\widehat{\xi}^2 - \sigma^2)/(\widehat{\xi}^2 + 2\sigma^2\widehat{\xi})$. An example is the linear distribution in Fig. 2.2, for which the variance is clearly very low: all particles see essentially the same distribution everywhere. Notice also that σ_c^2 tends to zero when the cell size approaches the universe size, that is when the sample is larger than the scale of homogeneity.

The fact that the variance for a fractal is large is a crucial aspect of the whole question of comparing fractals to the real world. All quantities, like the correlation function and the power spectrum, which are normalized with the conditional density, are subject to a variance in amplitude which can be as large as 100% and more. Therefore, all tentative of rejecting fractals on the ground of the *amplitude*, like comparing the fractal r_0 or σ_8 to the observations, is deemed to be inconclusive. For instance, the expected value of r_0 in a survey of depth $R_s = 100$ Mpc/h for a $D = 2$ fractal is, according to Eq. (5.84), $r_0 = R_s/3 \simeq 33$ Mpc/h; the observed value in several surveys, however, is $r_0 = 5 \div 10$ Mpc/h . Because of the large variance, this discrepancy does not rule out fractals; a low value of r_0 is compatible with the expectation value $R_s/3$.

Then, how can we confirm or reject fractals? There is only a way of comparing significatively fractals to real distributions: using the *exponents* rather than the amplitudes, that is the *slope* of the correlation function, or of the power spectra and related quantities. Naturally, the samples to be employed must not be weighed according to some prescription which assumes homogeneity, as when a weight is assigned in magnitude-limited samples by using a luminosity function derived assuming homogeneity (see next Section for an example of this).

Let us consider some equivalent ways of testing fractals through slopes. The behavior k^{-D} of the power spectra is a clear and unambiguous signal of fractality, as long as it is found at scales quite smaller than the depth of the sample. The existence of a turnaround at these small scales, on the other hand, would definitively prove the approach to homogeneity.

A related slope test is the behavior of the conditional density at distance r averaged around each particle in the sample, or its integral in spherical cells (see Eq. (5.18))

$$\begin{aligned} \langle \rho_c \rangle &= \Gamma(r) \sim r^{D-3} \\ \langle \rho_c \rangle_{sph} &= \Gamma^*(r) \sim r^{D-3} \end{aligned} \tag{5.90}$$

Since these statistics are evaluated in spherical cells, and do not make use of the sample conditional density, they are unambiguous estimator of fractality. If $\Gamma^*(r)$ flattens as r^0 at some scale, then homogeneity is reached. This test has been extensively performed on many datasets, as we will show later on. A similar behavior is expected for the conditional density within a distance r from the observer alone (or radial density), without averaging over other particles. This allows to reach the largest depth in the survey, but the signal is much less stable due to the absence of the average over the observers.

An important comment is in order here. From Eq. (5.18), we see that $\Gamma^*(r) = \rho_0(1 + \widehat{\xi})$, where (see Eq. (5.42))

$$\widehat{\xi} = \int \xi(x) W(x) d^3x \tag{5.91}$$

Suppose now the window function $W(x)$ is a function of the spherical coordinates r, φ, θ that can be separated as

$$W(x) = W(r) W(\Omega) \tag{5.92}$$

where Ω is an arbitrary function of the angles. The usual normalization writes now $\int W(r) r^2 dr = \int W(\Omega) d\Omega = 1$. Then we can write the integral in (5.91) as

$$\widehat{\xi} = \int \xi(x) W(r) r^2 dr = \frac{3}{R_s^3} \int_0^{R_s} \xi(r) r^2 dr \tag{5.93}$$

which is independent of the angular part of the window function. Then, the conditional density can be estimated also when the survey is not a complete sphere, which is often the case. However, if the window function cannot be separated, the value of $\widehat{\xi}$ will depend on the specific form of the window, and the formulae based on radial integration, as Eq. (5.85), are no longer valid. Whenener the sphere in which $\Gamma^*(r)$ is calculated crosses the boundaries of the survey, this situation is likely to occur. Therefore, when estimating $\Gamma^*(r)$, care must be taken that the cells are all spherical, or, more generally, that they are always in the separable form (5.92). Taking only spherical cells simplifies the problem, but reduces the scale range, as we will see in the next Section. Notice

that there is not such a problem for $\Gamma(r)$, because a thin shell is by definition in the form (5.92) unless some non-trivial weighing scheme is assumed.

A similar comment concerns the estimation of σ^2 , often used to normalize the power spectrum to real surveys. While the definition (5.52) is general, the expression (5.53) $\sigma_8^2 = (2\pi^2)^{-1} \int P(k) W_8^2(k) k^2 dk$ holds only for complete spherical cells. For cells that cover less than 4π of sphere, the effective window function is wider, and the variance is larger, as expected. Since σ^2 enters in the variance of the conditional density, we see that, while the expected value of the conditional density remains the same in portions of spheres that cover less than 4π, its variance increases.

The fractal nature of a distribution can be confirmed or rejected also comparing the variation of the clustering amplitude, e.g. the value of σ_8 , with the depth in samples *around the same observer*, i.e. ourselves. In fact, the high variance we mentioned above is an ensemble variance, that is, is the variance for independent samples around different observers. If we investigate samples of increasing depth from the same observer, on the other hand, the variance has to be much smaller (although an analytical determination is difficult and it is easier to compare with simulations), because the samples are not independent. In this way, the expectation for a fractal is that the amplitude of σ_8 grows with sample size as R_s^{3-D}. Another possibility, related to this one, is to see whether the normalization-independent relation $r_0 = 2^{1/(3-D)} r_c$ holds for various samples.

All these tests are of course mathematically related, and the only parameter is the fractal dimension, and possibly its variation with scale. In the next Chapter we will focus on tests based on slopes.

3.3.5 The fractal dimension of CDM models

We have remarked already that any inhomogeneous distribution can be described as a fractal at least in some range of scales. Let us see then what kind of fractal can approximate the CDM-like models.

The fractal dimension of a distribution characterized by a spectrum $P(k)$

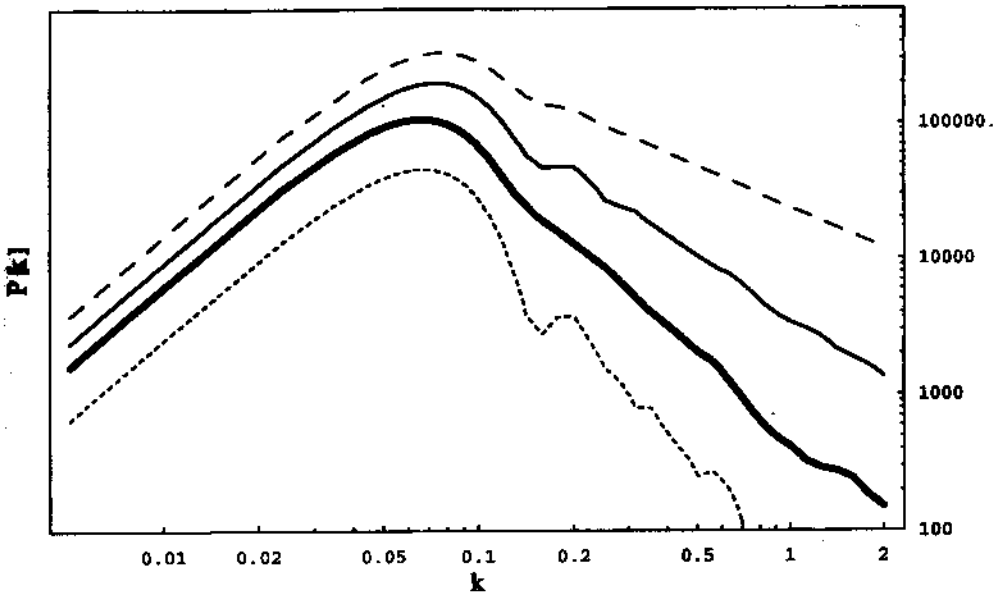

Figure 3.8: **Power spectrum of fractals for $D = 1, 1.5, 2, 2.5$ top to bottom.**

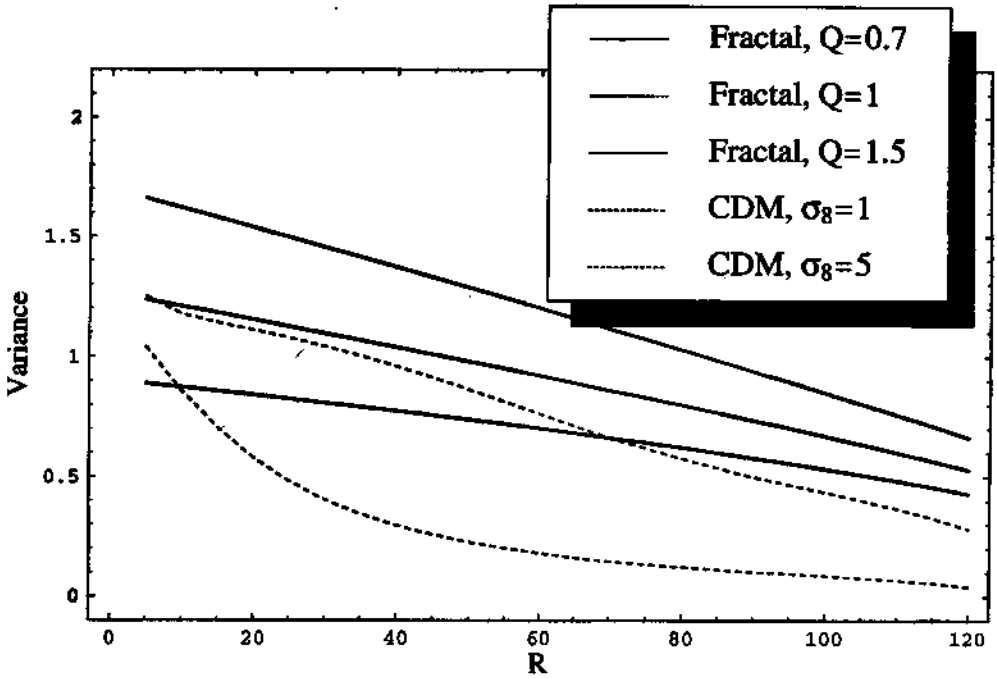

Figure 3.9: **Percentual variance for some models of fractal with cut-off and of CDM. In all cases, at scales small compared to the homogeneity scale the variance is 100% or more of the expected value of the conditional density. For a standard CDM, the variance goes to zero (neglecting the Poisson noise) around 50 Mpc/h.**

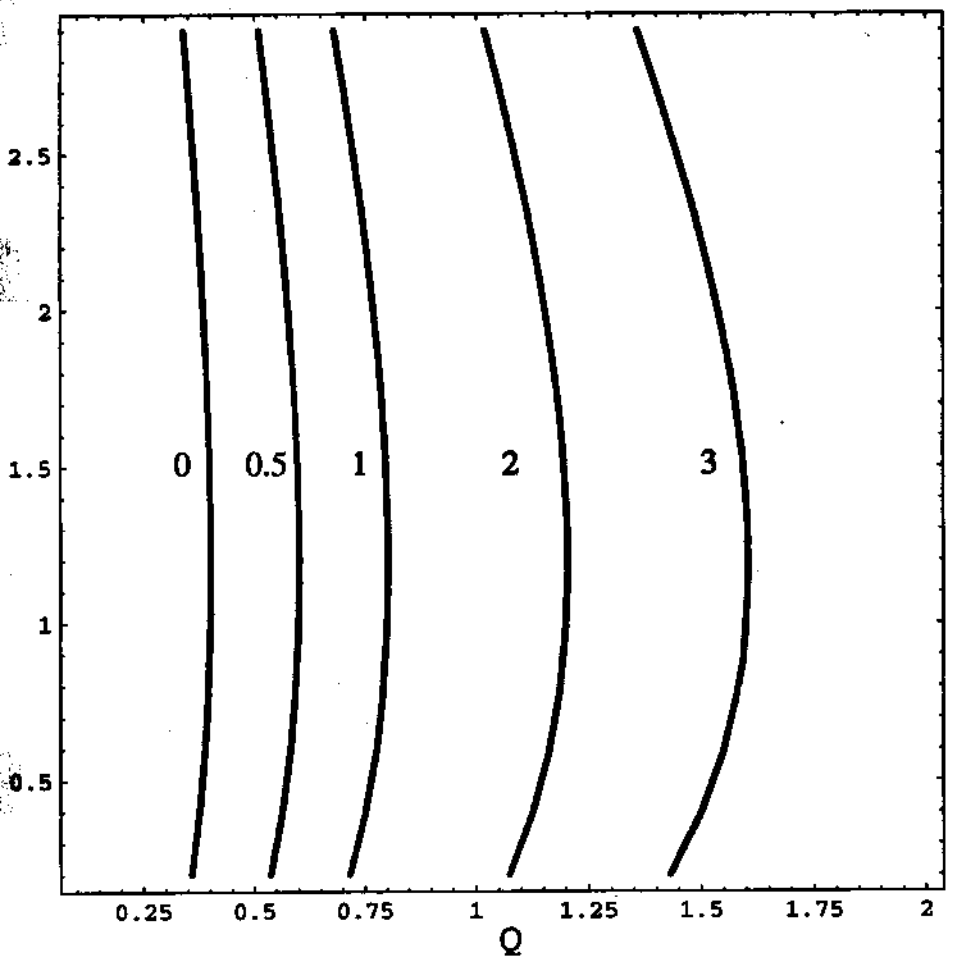

Figure 3.10: **Contour plot of the percentual variance in the (D, Q) plane for a fractal in the limit of small scales. Reasonable values of D, Q give a variance of 100% or larger.**

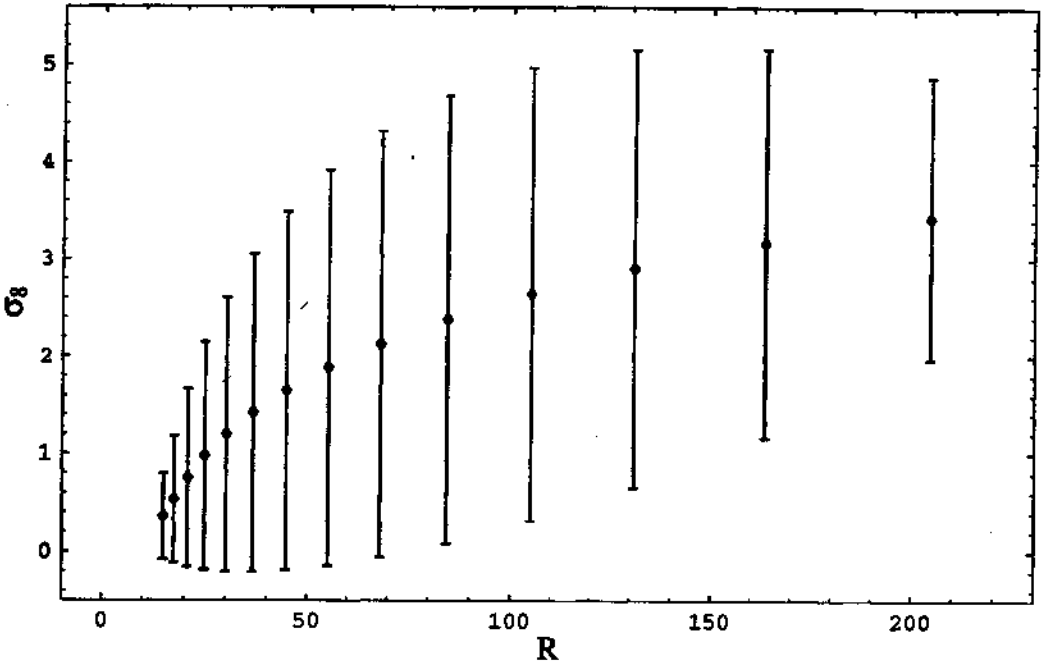

Figure 3.11: **Normalization σ_8 for a fractal with cutoff at 300 Mpc/h. The ensemble variance is so large that a very wide range of σ_8 is allowed.**

is, by Eq. (5.80)

$$D(R_s) = 3 + \frac{d\log(1+\widehat{\xi})}{d\log R_s} = 3 + \frac{\int P(k)W'(kR_s)k^2dk}{(2\pi^2) + \int P(k)W(kR_s)k^2dk} \qquad (5.94)$$

where $W' = R_s dW/dR_s$. We can immediately infer some properties of the function $D(R_s)$. First, if $\xi(r)$ decreases with r, then $D(R_s)$ is smaller than 3. Secondly, in the limit of large spectrum amplitude, the fractal dimension becomes independent of the amplitude itself.

It is clear that an effective, scale-dependent fractal dimension can be defined for any given power spectrum. In this sense, the single-law fractal is just an extreme model among a continuous class of inhomogeneous models. From this point of view, the only one which is relevant to our discussion, the difference between CDM and fractals is purely quantitative. The same physics of gravitational instability that explains CDM can explain a fractal behavior up to some scale. In the standard cosmology, this scale will be set by the amount of initial fluctuations and by the amount of time the structures are allowed to grow. Different initial conditions can lead to a different scale of homogeneity.

Let us see now whether there is a range of scale in which $D(R_s)$ for a CDM spectrum is approximately constant. In Fig. 3.8 we display the fractal dimension versus sample size for some standard CDM models, with various normalizations, corresponding to COBE (total matter), to average galaxies, to bright galaxies, to clusters, with and without redshift correction. In general, the CDM models with redshift correction have a fractal dimension between 2 and 2.5 up to 50 Mpc/h, and homogenize afterward. It is the fact that $D(R_s)$ is almost constant in this range that makes the fractal mathematics useful also for standard models. In the same figure the behavior of the conditional density in samples of size R, i.e. $\Gamma^*(R)$, is also shown. The flattening of $\Gamma^*(R)$ indicates homogeneity, i.e. the distance at which the sample density approaches the universe density. Notice that even the standard model flattens only beyond 50 Mpc/h.

The scale at which the dimension goes to 3 increases with the power spectrum normalization, as expected. If we define the scale of homogeneity as the scale λ_h at which $D(R_s) = 2.9$, then we can find a simple approximate relation between λ_h and the normalization σ_8 assuming a shape parameter $\Gamma = 0.2$, without redshift correction (to include it, it is sufficient in a first approximation to replace σ_8 with $\sigma_8 f(\beta)^{1/2}$)

$$\lambda_h = 25\sigma_8 \mathrm{Mpc/h} \qquad (5.95)$$

For instance, if $f(\beta) = 2$ and $\sigma_8 = 1.7$, as observed for bright galaxies in SSRS2 (Benoist et al 1996) the homogeneity scale could be as large as 60 Mpc/h. For clusters, the scale can be larger than 70 Mpc/h. Because of the small-scale non linearity, which increases the clustering level, these values can even be pushed somewhat further.

Below the scale of homogeneity the distribution of galaxies behaves like a fractal: that is, its power spectrum amplitude increases with the sample size, has a large variance, and the spectrum turns around at the scale of

the survey depth. In Figure 3.9 I show CDM spectra estimated in samples smaller that the scale of homogeneity, where these effects are clearly shown. The determination of the scale of homogeneity is therefore crucial. The first consideration is that the scale of homogeneity cannot be determined from σ_8 estimated from a single finite survey. The σ_8 in (5.95) is the universe value, not the sample value. From the power spectrum in a finite survey we have

$$\sigma^2_{8,s} \simeq \frac{\sigma^2_8}{(1+\widehat{\xi})} \tag{5.96}$$

where the approximate equality holds for $R_s \gg 8$ Mpc/h. That is, once again, the normalization in finite samples is lower than the true normalization, unless we are on scales such that $\widehat{\xi} = 0$. Then, the values of $\sigma^2_{8,s}$ obtained from galaxy surveys are only a lower limit to the true normalization. To constrain the true value, we have first to verify that $\widehat{\xi}$ already approached unity by detecting either the turnaround in the spectrum or by detecting a trend toward a constant of $\sigma^2_{8,s}$ in various samples of larger and larger depth. I will argue in the next Section that this is still to be found without ambiguity.

Notice that the value of σ_8 deduced from the microwave background experiments is a universe value. In this case, the scale of homogeneity is really small, of the order of 25 Mpc/h. However, we have to keep in mind how many assumptions are implicit in this determination, for instance that gravitational instability is the only mechanism for structure formation, and that the CDM spectrum shape is accurate. Moreover, this value of σ_8 applies to the total matter; galaxies and clusters could be strongly biased tracer of mass.

Since a CDM-like distribution, as any other distribution, is a fractal when it is seen in samples smaller that the homogeneity scale, from now on I will say that a distribution is fractal when *the sample is smaller than the homogeneity scale*, and is homogeneous *when the sample is larger*. Once we accept this point of view, the property of fractality or of homogeneity can be seen as *a property of the sample geometry*, rather than an intrinsic property of the distributions. Once again, the only question that makes sense is: have we already reached the homogeneity scale?

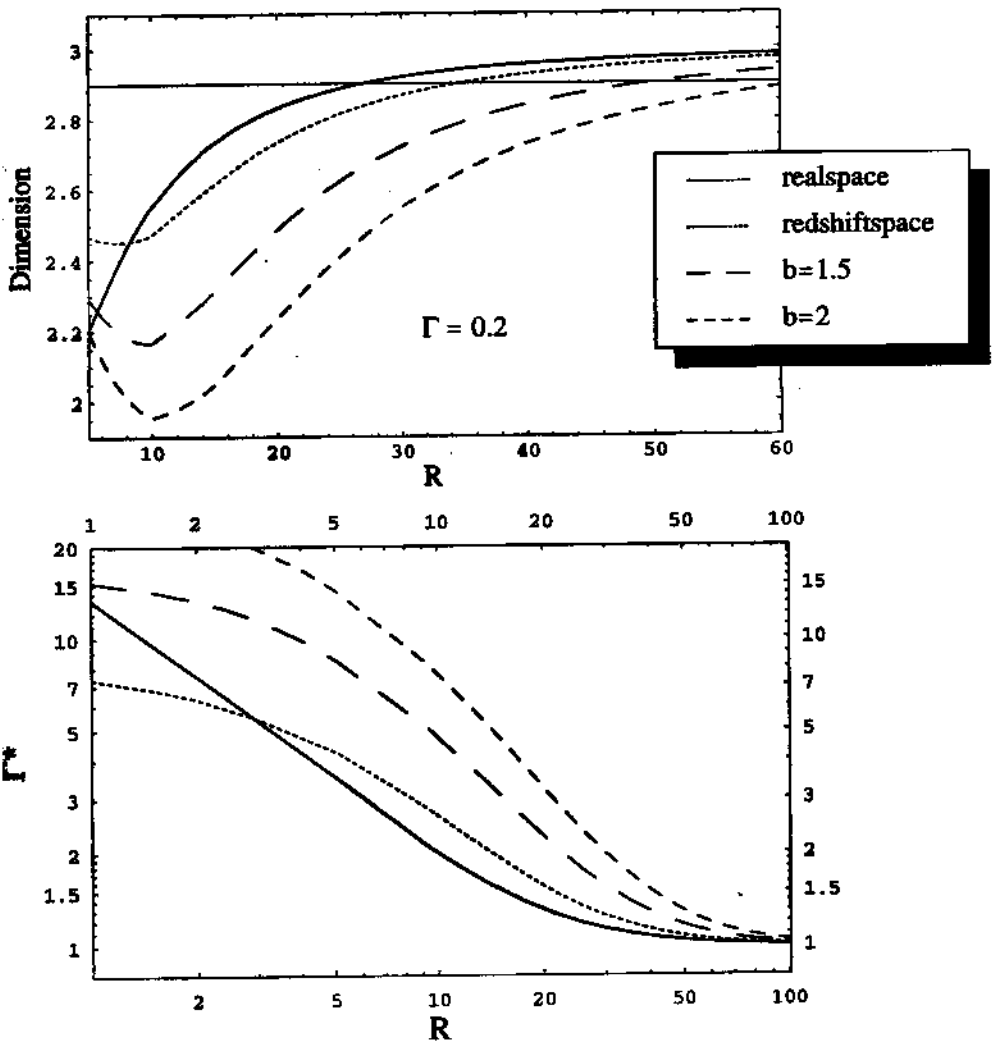

Figure 3.12: **Top: Effective fractal dimension for CDM models with shape parameter $\Gamma = 0.2$ and various normalizations. A range of almost constant dimension is found at small scales when the spectrum is redshift corrected. At scales below 10 Mpc/h the linear spectrum we are using should be corrected for the non-linear growth. Bottom: $\Gamma^*(r)$ for the same models.**

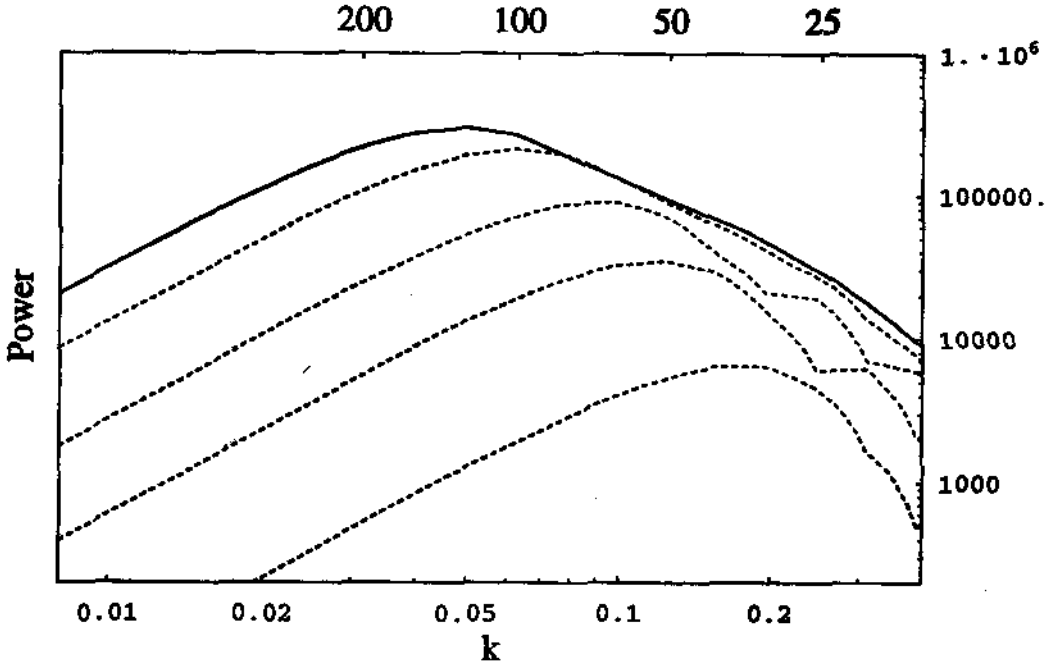

Figure 3.13: **The CDM spectrum with a high normalization, $\sigma_8 =$ 3 , estimated in finite samples of size 25, 50, 100, 200 Mpc/h. Only the largest samples give an accurate estimate, both in terms of amplitude and of shape.**

3.3.6 Other predictions

We briefly review here some other predictions of the fractal model, to be compared with the homogeneous case: the number counts, both as a function of distance and of magnitude, and the angular correlation function. Any of these predictions can be tested, at least in principle, so as to derive bounds on the homogeneity scale. However, we will focus in the following mostly on the power spectrum and related quantities, because they give the highest quality information on the real distribution of galaxies in space.

The most direct prediction of a fractal distribution is the density scaling law Eq. (5.78). However, in a magnitude-limited survey, the density scaling law is modified by the selection procedure. In a sample of depth R and volume V that contains all galaxies with an apparent luminosity brighter than m_1 and fainter than m_2, the density of galaxies will be

$$n(R) = V^{-1} \int_0^R \rho_c(r) r^2 dr \int_{M(m_1,r)}^{M(m_2,r)} \phi(M) dM \tag{5.97}$$

where $M(m,r) = m - 5\log r - 25$ and $\phi(M)dM$ is the luminosity function which, as usual, can be written as the Schechter function

$$\phi(M) = \phi_0 \exp[-10^{0.4(M^*-M)}] 10^{0.4(M^*-M)(\alpha+1)} \tag{5.98}$$

Since the samples can extend fairly deep, it is necessary to take into account the relativistic effects and the K-correction. If $f(\nu)$ is the flux at the observer in the wavelength ν, and L the absolute luminosity of the source, we have

$$f = \frac{L}{4\pi r^2 (1+z)^{1-\alpha_k}} \tag{5.99}$$

where α_k is the spectral index of the source,

$$\alpha_k = \frac{d\log f}{d\log \nu} \tag{5.100}$$

The observed apparent magnitude is $m = -2.5\log f$. The K-correction is embodied in the factor $(1+z)^{1-\alpha_k}$. For optical galaxies, the usual term kz in the distance modulo is approximated by $\alpha_k = -1 - k/2.5$. Values often quoted in literature for the various spectral bands are: $\alpha_k = -2.2$ for optical galaxies; $\alpha_k = -0.7$ for radiogalaxies; and $\alpha_k = -0.5$ for quasars and for r-band selected galaxies (Lin et al. 1996). Then, the general expression can be written as

$$n(z) = \rho_0 V^{-1} R^{3-D} \int_0^{z(R)} r(z')^{D-1} f(z') dz' \int_{M(m_1,z')}^{M(m_2,z')} \phi(M) dM \tag{5.101}$$

where

$$M(m,z) = m - 5\log[(1+z)^{1-\alpha_k} r] - 25 \tag{5.102}$$

and, for $\Omega_0 = 1$,

$$r(z) = 2H_0^{-1}[1 - (1+z)^{-1/2}] \tag{5.103}$$

and finally $f(z) = dr/dz$. Denoting with $N(>f)$ the number of galaxies with flux larger than f, i.e.

$$N(>f) = \lim_{z\to\infty} V(z)n(z)$$

we see that for small z, i.e. large fluxes f, one has $r = z/H_0$, and this gives the Euclidean fractal result $N(>f) \sim f^{-D/2}$, independently of $\phi(M)$. At large z, on the contrary, we have $N(>f) \sim f^0$, again independently of $\phi(M)$. We can say then that the *apparent* fractal dimension $D_a = -2[d\log N(>f)/d\log f]$ declines from the real dimension D at large fluxes to 0 at small fluxes (more exactly, $D_a(f\to 0) = f^{1/2(1-\alpha_k)}/(\alpha_k - 1)$).

Eq. (5.101) can also be written as a function of the limiting magnitude of the sample, i.e. as $n(m_{\rm lim})$. Then we have, in the limit of large fluxes

$$\frac{d\log N(m)}{dm} = \frac{d\log N(>f = 10^{-0.4m})}{dm} = \frac{D}{5} \tag{5.104}$$

instead of the usual slope 0.6 valid for the homogeneous case in the Euclidean $D = 3$ limit. A comparison of fractals to real data is in Sylos-Labini, Montuori, Gabrielli & Pietronero (1996).

Finally, let us investigate the fractal behavior of the angular correlation function. The predictions for the angular correlation function is contained in Eq. (5.27) for small angles and for a power-law spatial correlation. Putting $\xi(r) = Ar^\gamma$ with $A = (D/3)R_s^\gamma$ we obtain $w(\theta) = B\theta^{1-\gamma}$, where, for a selection function equal to unity up to the scale R_s and zero afterwards

$$B = 2R_s^{-6}AH_y\int^R x^{5-\gamma}dx = 2(D/3)H_y\int_0^1 y^{5-\gamma}dy \sim const$$

that is, the correlation function does not depend on the depth R, contrary to the homogeneous case. The same happens for other selection functions with a typical scale R_s. The angular correlation function should then remain constant also as a function of the limiting magnitude, at least in the Euclidean, small angle limit. The angular function of the APM catalog (Maddox et al. 1990), on the contrary, decreases with the limiting magnitude, in agreement with the homogeneous prediction. However, a direct comparison with real fractals, including relativistic and evolutionary effects, is still to be done (the data are not yet publicly available). Moreover, the usual practice in such analyses is to remove large scale angular gradients, attributed to calibration errors; needless to say, this procedure would destroy intrinsic large scale inhomogeneities. Finally, the angular correlation function is dominated by distant objects, so that the scaling can prove at most that some large homogeneity scale do exist.

3.4 Observations

3.4.1 Introductory remarks

This Section is devoted to the systematic comparison of some observations with the alternative predictions of standard CDM models and of fractal behaviors. I will mostly focus on the determination of the 3-dimensional power spectrum, because the 3D catalogs give the maximum information on the real galaxy distribution, and because the near future production of deep redshift surveys will allow a more precise assessment of the effects I will mention here.

The first thing to make clear is that we will investigate mostly volume-limited (VL), rather than magnitude-limited (ML) samples. The latter are samples which selects all galaxies brighter than some apparent magnitude limit, $m_{\rm lim}$. Clearly, the larger the distance, the brighter a galaxy has to be in order to be included. Therefore, in a ML sample, the density will show an apparent decrease with depth because more and more galaxies will fall below the threshold for detection. Only a precise knowledge of the luminosity function allows one to weigh correctly this apparent decrease. The problem is, that the LF itself is often estimated from ML samples assuming that the sample is homogeneous, and therefore it cannot be used to test the real density scaling that may be present in the data. For instance, as we will see below, in the case of the Las Campanas redshift survey, the LF has been fitted to the data assuming that the distribution is homogeneous (in Lin et al 1996a), and then the same LF is used in, e.g., Lin et al. 1996b, and Tucker et al. (1996) to weigh the distribution in order to determine the power spectrum or the correlation function. As we will see, however, the initial assumption of homogeneity is by no means justified by the data themselves, and a dimension $D = 2$ is equally well consistent with the data.

The way to distinguish between an apparent decrease due to luminosity and a real decrease due to density scaling is to analyze volume-limited samples. A volume-limited sample selects only the galaxies within a distance R which are intrinsically bright enough to be included in the sample even if were exactly at distance R, i.e. at the boundary of the sample. In this way, any density trend within the sample is to be attributed entirely to a real scaling, rather than to the apparent magnitude effect.

A volume-limited sample has the drawback that it discards a large portion of the data. However, one can study several VL samples, at different depths, so most of the data can still be exploited. On the other hand, the various subsamples contain galaxies of different magnitude, so that any difference between one and the other could be attributed to a luminosity segregation rather than to a density effect (see Fig. 4.1). Since brighter galaxies are expected in the model of biased formation to cluster more strongly than fainter ones, the two effects have the same qualitative behavior.

This point is crucial to the interpretation of some of the data we are going to present: any trend in VL samples can be interpreted both in terms of density scaling (fractal), or in terms of luminosity segregation. This is the main reason why the same datasets have been interpreted sometimes as confirming both the fractal and the homogeneous view. There is however the possibility of disentangling the two effects.

First, the fractal behavior depends only on D, so that the slope of the power spectrum and the amplitude increase are related, and are not independent as when the effect is due to the luminosity segregation. Secondly, we can further cut the VL samples in subsamples with the same magnitude limits, and different distances, or with the same distances and different magnitude limits, and test the effects separately.

Some of these tests have been done in literature. However, as I will argue, they have been inconclusive so far, both because there is no precise prediction on what the luminosity segregation has to be, and because the data are not rich enough to allow for further cuts. Also, the brighter galaxies could have a different fractal dimension than fainter ones, so that the fractal trend can become complicated.

3.4.2 A collection of old data

Many galaxy surveys produced a correlation function $\xi_s(r)$ which goes as $r^{-1.8}$ on scales less than 10 Mpc/h. This could imply a fractal dimension $D \simeq 1.2$ on such scales, but the approximation of $\xi_s(r)$ with a pure power-law is not a good way of testing for fractality, since is $1 + \xi_s(r)$ which is expected to be a power-law, and not $\xi_s(r)$. Moreover, $\xi_s(r)$ is expected to become negative at $r_c \simeq 2r_0 \simeq 10$ Mpc/h (see Sect. 3.2), so that $\xi_s(r)$ is rarely studied beyond this distance; then, no information is provided about the scales on which the CDM and the fractal predictions differ, that is well beyond 30 Mpc/h.

More useful is the statistics $\Gamma(r)$ introduced in Sect. 2.3, that is the average conditional density seen from any galaxy. When it is estimated in spherical shells, it does not introduce spurious couplings with the sample geometry, contrary to $\xi(r)$ or $P(k)$, so that its power-law trend as r^{D-3} is an unambiguous probe of fractality. When the scale of homogeneity is reached, a plateau has to be detected, $\Gamma(r) \sim const.$ The same holds for the integral in spherical cells, $\Gamma^*(r)$, with smaller variance.

Pietronero and coworkers have analyzed in the past years essentially all the datasets publicly available (Pietronero, Montuori & Sylos Labini 1997, Sylos-Labini, Montuori & Pietronero 1998). Their results are summarized in Fig. 4.2. Since $\Gamma^*(r)$ has to be evaluated in full spheres centered on galaxies, the largest scale one can reach is the radius of the largest sphere that fits

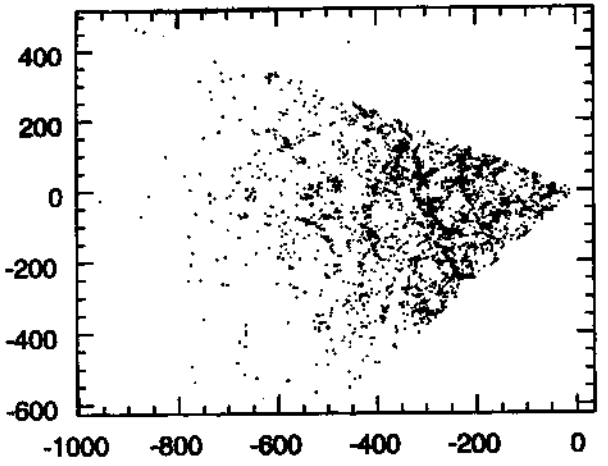

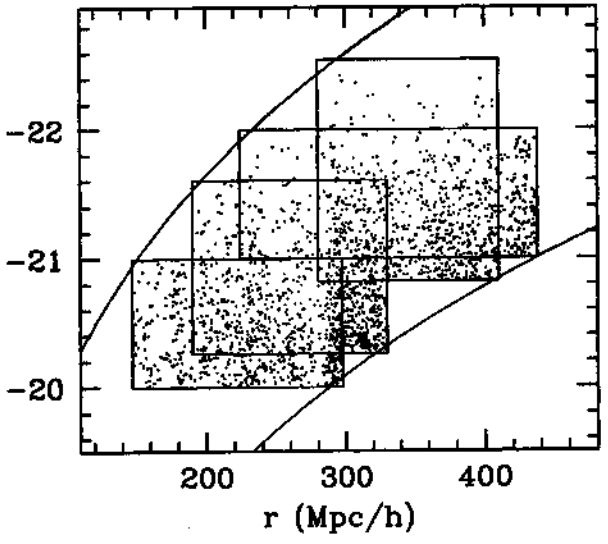

Figure 3.14: **A slice of the Las Campanas redshift survey and, below, some of its volume-limited samples. The Las Campanas has a lower and a upper limiting apparent magnitude. Then, the volume-limited samples require an inner and an outer cut in distance (Palladino 1997).**

in the survey, and at this scale the error is large because the average can be done on few spheres. Actually, it is possible to perform this calculation also in portions of spheres, as we will show below, so as to extend the range. We see from Fig. 4.2 that the data show a $D \simeq 2$ fractal behavior from 1 to 30 or 40 Mpc/h. This indicates that the scale of homogeneity is certainly larger than this. In the same Fig. 4.2 the data that extends to 100 Mpc/h come from the Leda redshift database (Paturel et al. 1994; Di Nella et al. 1996) . However, the Leda database is incomplete at large distances, so that these results are not entirely reliable.

Notice that here there is no question of luminosity effects: each VL sample is analyzed on its own. This is certainly the simplest and less ambiguous test for fractality one can make.

3.4.3 CfA

The redshift survey CfA2 includes ~11000 galaxies with $m \leq 15.5$, in roughly one quarter of the sky. There are 6478 galaxies in the North hemisphere and 4283 in the South one. In Park et al. (1994) the power spectrum and the correlation function has been calculated for the whole ML sample, and for two VL samples, one cut to 130 Mpc/h, including 608 galaxies brighter that -20.3, the other cut at 101 Mpc/h,with 1509 galaxies brighter than -19.7. The resulting spectrum is reported in Fig. 3.2.

The spectrum shows several interesting features:

- The spectrum rises as k^{-2} for scales smaller than 30 Mpc/h, and flattens to k^{-1} afterward.
- The spectrum of the deeper and brighter sample is 40% higher than the shallower and fainter one.
- There is a tendency to peak around 100-150 Mpc/h, although the errorbar is quite large at these scales.

All these features are consistent both with a CDM-like model, with luminosity biasing, and with a fractal spectrum with $D \simeq 2$. In Figs. 4.3 we plot the data along with some CDM and fractal spectra (Sylos-Labini & Amendola

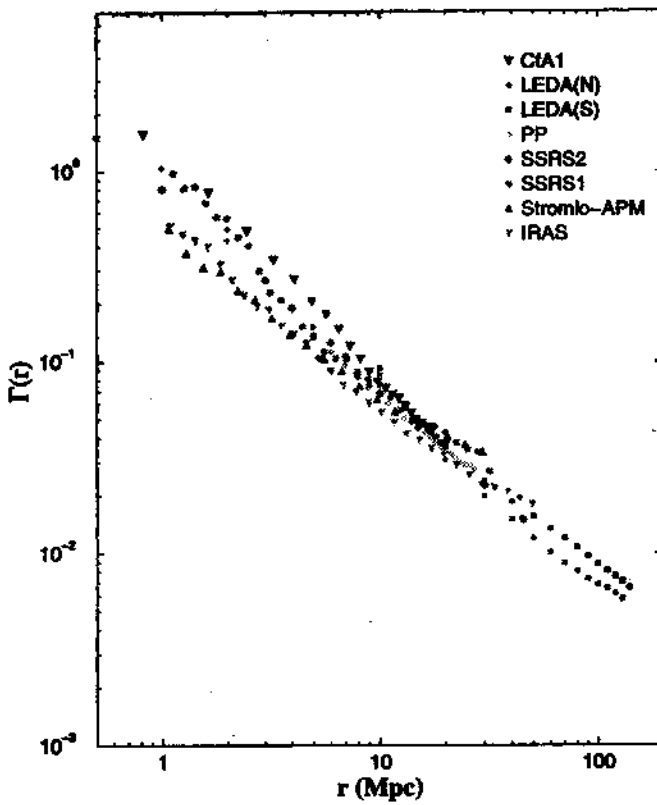

Figure 3.15: The function $\Gamma^*(r)$ for several samples (courtesy of F. Sylos-Labini).

1996). In the standard CDM-like interpretation, the increase in amplitude is due to the higher clustering of the brighter galaxies, and the spectrum peak, although not statistically significant, is what is expected from the theory. In the fractal interpretation, the amplitude shift is a consequence of the conditional density scaling, and the spectrum peak is a consequence of the window function. At the present status of the data, it is not possible to distinguish between the two interpretations. In the original Park et al. (1994) paper, no clear evidence of luminosity biasing was found, except for some part of the lower luminosity spectrum (at 60 and 78 Mpc/h). We examined data taken from the public Leda database, in the same region as the CfA2 data, containing roughly 70% of the galaxies in CfA2, and found evidence for true density scaling, rather than luminosity biasing, from 60 to 130 Mpc/h (Amendola et al. 1997). As already mentioned, however, the Leda database is incomplete, so that it is difficult to draw convincing results from it.

3.4.4 SSRS

SSRS2 includes 3600 galaxies in 1.13 sr of the southern sky, down to an apparent magnitude of 15.5. The power spectrum of SSRS2 (Da Costa et al. 1995) is very similar to the one of CfA2, and shows the same scaling between the volume-limited samples at 101 and 130 Mpc/h. The analysis presented for CfA2 can be applied therefore to SSRS2 as well.

In another paper, Benoist et al (1996), the SSRS2 data were partitioned in many volume-limited subsamples, in order to look for luminosity biasing. The correlation function was calculated in 9 VL samples cut at various depth, from 30 to 168 Mpc/h. The function exhibits an amplitude scaling of roughly a factor 3 or 4. The normalization r_0, defined in Eq. (5.84), increases from 3-4 Mpc/h, to 16 Mpc/h in the deepest sample, in rough agreement with the linear scaling expected from Eq.(5.84). The results were interpreted as an evidence of luminosity bias, because the smaller samples contain galaxies brighter than -17, while the deepest sample galaxies are brighter than -21. However, to distinguish between luminosity bias and density scaling it is necessary to partition the same VL sample into smaller subsamples at various depth and similar magnitude cuts. In this way, the samples become extremely poor (the VL samples considered above contained as few as 67 or 105 galaxies in

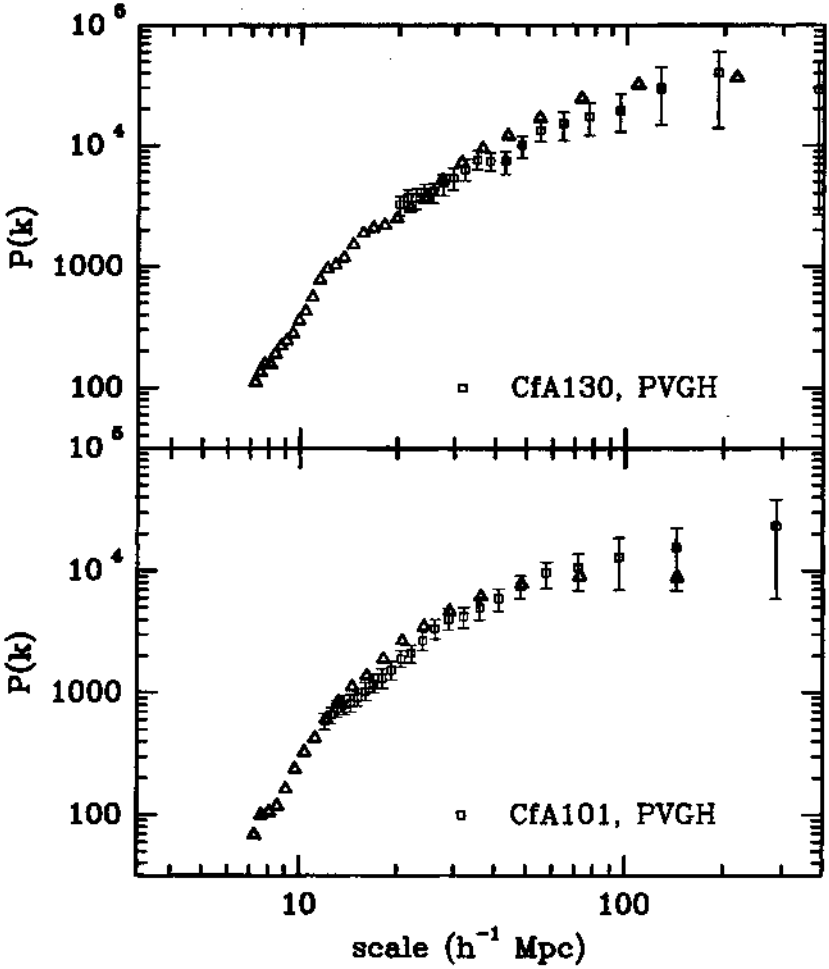

Figure 3.16: **The CfA2 data compared with two fractal simulations with the same geometry of the real data (from Sylos-Labini & Amendola 1996).**

some cases, that is a mean separation of 15 Mpc/h). Due to the large errorbars, then, the conclusions drawn in Benoist et al. (1996), therefore, are again inconclusive, and are compatible both with fractals and standard scenarios.

In Cappi et al. (1998) the question of fractality has been considered in greater detail, using the same SSRS2 data. The conditional density $\langle \rho_c \rangle$ has been evaluated in spherical cells and shells, in order to produce the statistics $\Gamma(r)$ and its integral average, $\Gamma^*(r)$. The result is that the conditional density decreases as r^{-1} from 1 to 50 Mpc/h in all the VL samples considered, implying fractality with $D = 2$ on these scales, with no indication of flattening. These are the largest scales that can be probed via this method. The conditional density from the observer alone, i.e. from the vertex of the sample, has also been studied, in order to extend the range. The results are that the sample is fractal up to 50-80 Mpc/h and tend to homogeneity above this scale. However, the errors are quite large; within 2σ the deepest samples include all values between $D = 2.7$ and $D = 4$. The errors quoted, moreover, do not include the ensemble variance that, for fractals, is very large, as already mentioned. This can be estimated only by comparing with simulated fractals, because the samples are not independent. My conclusion is that the SSRS2 data prove fractality up to 50 Mpc/h, roughly, and have not enough data beyond this scale. The values of $\sigma_{8,s}$ estimated in the sample are consistent with this interpretation: they are larger than 1.3 for the largest samples, which implies in redshift space $\lambda_h > 50$ Mpc/h.

3.4.5 Las Campanas

The Las Campanas redshift survey, LCRS, contains 23,697 galaxies with an average redshift $z = 0.1$, distributed over six $1.5^0 \times 80^0$ slices in the north and south galactic caps.

The survey contains fields which includes galaxies with magnitude between 16.0 and 17.3 , and fields with limits 15.0 and 17.7. Every field has associated a filling factor $0 < f < 1$ which is the fraction of the galaxies randomly chosen out of the total number in the field within the magnitude limits. The inverse of f is therefore a weight to all galaxies in that field, and must be taken into account in the statistics.

Lin et al. (1996) evaluated the power spectrum in the whole magnitude-

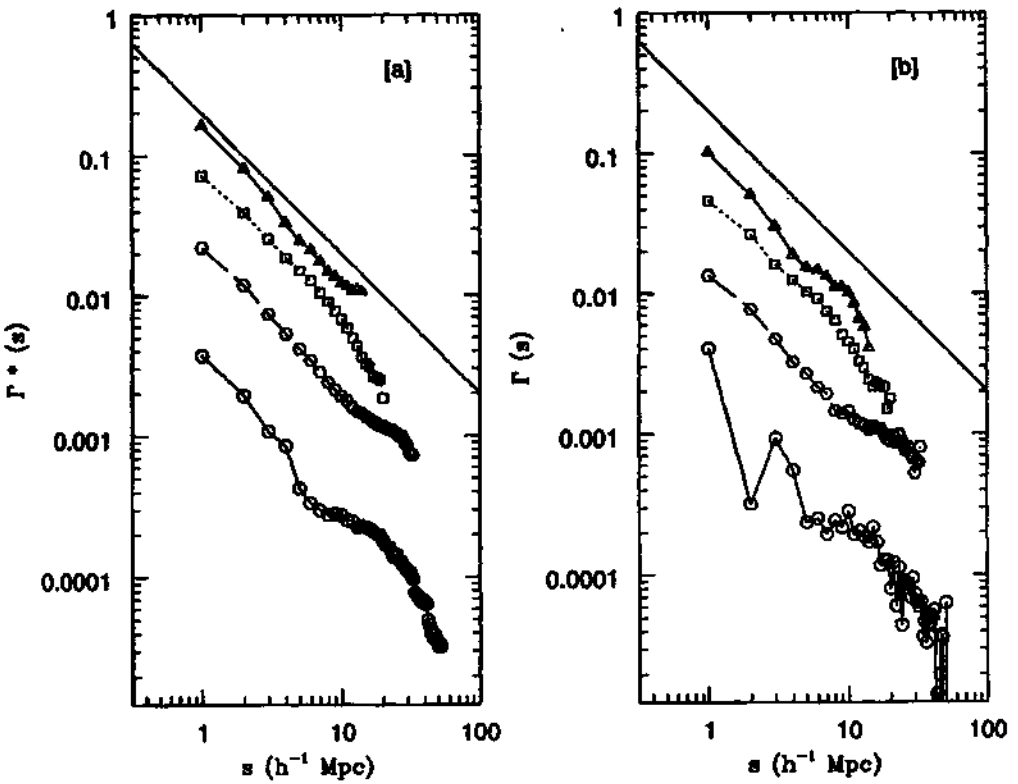

Figure 3.17: **The function $\Gamma^*(r)$ and $\Gamma(r)$in various VL subsamples of SSRS2 (from Cappi et al. 1998)**

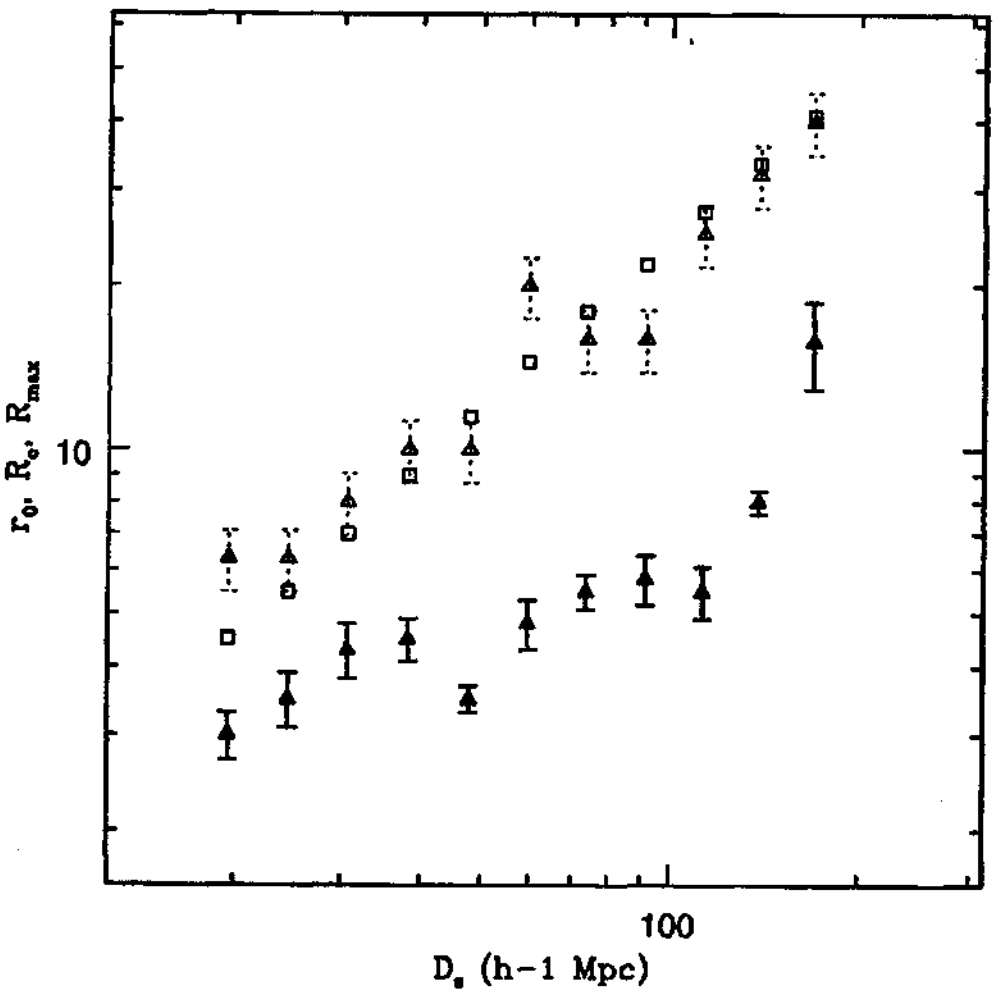

Figure 3.18: **Values of r_0 and r_0 in VL samples of SSRS2 (from Cappi et al. 1998)**

limited sample adopting the luminosity function estimated by assuming homogeneity, so that this spectrum cannot be used to investigate the fractal model. They also evaluated the PS in volume-limited subsamples, but the existence of two magnitude limits makes difficult to compare with a theoretical fractal. In any case, they find again an increase of power with increasing depth and magnitude, but the errors do not allow any conclusion to be drawn (see their Fig. 10).

We performed a very preliminary study of the conditional density in LCRS, using the only slice with fields of large magnitude range (slice at -12^0; Palladino 1997). We evaluated the conditional density integrated in cells with a shape and orientation such as not to intersect the survey boundaries (see Fig. 4.6, cells marked with R) . This avoids the effect of the window function in the statistics and allows to include pretty large scales. We cut the sample into four VL subsamples, delimited by a lower and an upper cut (this is necessary because LCRS has two limiting magnitudes). The samples are denoted VL147-297, VL 190-330, VL280-410, and VL224-437, where the numbers give the lower and upper cutoff distance (see Fig. 4.1).

The result for the $\Gamma^*(r)$ is shown in Fig. 4.7. It can be seen that there is a clear $D = 2$ fractality on small scales, up to 20 or 30 Mpc/h, just as in the SSRS2 case, followed by a flattening of the slope. The scales we reach here are the *largest scales ever reached* for the $\Gamma^*(r)$ statistics, more than two times the SSRS2 depth. In the case of VL280-410, the behavior is power-law, albeit with a change in slope, down to more than 100 Mpc/h, while for VL224-437 (the most sparse sample) a very noisy flattening is reached at 40 Mpc/h. The $\Gamma^*(r)$ erroneously calculated in non-radial cells (see Fig. 4.6, cells marked with NR) is systematically higher and reach an apparent homogeneity at shorter scales.

From these results we can conclude that there is a tendency to homogenization around 50-100 Mpc/h, as expected from a CDM model (e.g. with $\Gamma = 0.2$, redshift correction, and $\sigma_8 \simeq 1.5$). However, we remark that we did not detect a clear homogeneous behavior, that is $\Gamma^*(r) = const$, not even at more than 100 Mpc/h, except for the most sparse sample. This leaves again space for a fractal behavior to larger scales, although with a dimension closer to 3. The scale reached is critical: the CDM behavior is absolutely flat ($D \simeq 3$) beyond 100 Mpc/h. If we can go to a larger scale, either $\Gamma^*(r)$ stabilizes around homogeneity, or continues with the same slope, and a higher value of σ_8 would be required. A more precise comparison with CDM and fractal simulations is under way.

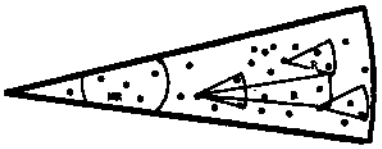

Figure 3.19: **The geometry of the cells used to estimate the conditional density in LCRS. Radial cells are marked with R, non-radial with NR.**

3.4.6 The number density in Las Campanas

The density of galaxies in a shell between $R_1 - \Delta/2$ and $R_1 + \Delta/2$ of volume V_R, in a sample of average density ρ_0, is by Eq. (5.101) :

$$\begin{aligned} n(R) &= V_R^{-1} \int_{V_R} \rho_c[r(z)] f(z) r(z)^2 dz \int_{M(m_1,z)}^{M(m_2,z)} \phi(M) dM \\ &= \rho_0 V_R^{-1} R^{3-D} \int_{V_R} r(z)^{D-1} f(z) dz \int_{M(m_1,z)}^{M(m_2,z)} \phi(M) dM \end{aligned} \quad (5.105)$$

For any given survey, characterized by m_1 and m_2, and any value of R, the density depends on D, M_* and α, once the other parameters (α_k and the cosmological parameters) have been fixed. In almost all the published literature the parameter D is fixed to the homogeneous value, $D = 3$, even when the sample is markedly inhomogeneous, and only the luminosity function parameters are fitted to the data. Here we want to fit at the same time the three parameters in the deepest redshift survey so far produced, the Las Campanas Redshift Survey.

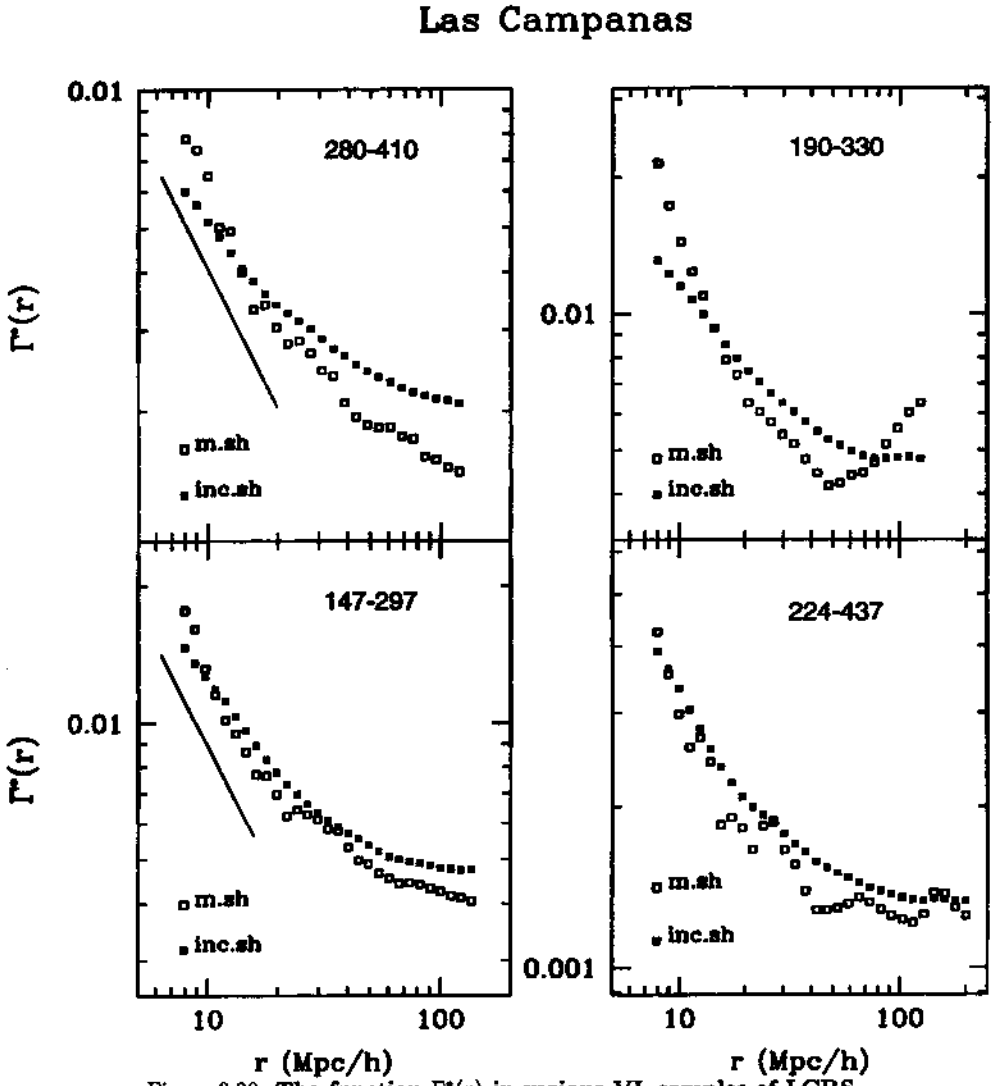

Figure 3.20: **The function $\Gamma^*(r)$ in various VL samples of LCRS. The open squares refer to the cells with radial geometry. The filled squares refer to cells with non-radial geometry: they give systematically a flatter behavior (from Palladino 1997).**

To do this, we adopt the likelihood function procedure. Let us divide the slice at -12^0 in m radial shells of equal thickness, and let n_i be the density of galaxies in the i-th shell. Then, if $n(r_i; D, M_*, \alpha)$ is the theoretical prediction, we can form the likelihood function

$$F = -2 \log L = \sum_i^m \left\{ [n_i - n(r_i; D, M_*, \alpha)]^2 / \sigma_i^2 + \log[2\pi\sigma_i^2] \right\} \qquad (5.106)$$

and maximize it with respect to D, M_*, α. We choose the cosmological parameters $\Omega = 1, \Lambda = 0$ and for the k-correction we adopt $\alpha_k = -0.5$, the same values adopted in Lin et al. (1996) who derived the LF for Las Campanas with the homogeneous assumption.

We take 25 slices of 25 Mpc/h each, down to 625 Mpc/h. Since visualizing the probability contours of $F(D, M_*, \alpha)$ is impractical, we display in Fig. 4.7 the contours in the plane D, M_* for $\alpha = -0.25, -0.7, -1$. The value $\alpha = -0.7$ is the one found in Lin et al. (1996) by assuming $D = 3$; the other values are within the range often found in literature (for instance $\alpha = -0.3$ is in Lin et al. by considering only emitting galaxies). The contours in Fig. 4.7 are for $\Delta F = 2, 10, 20$ which roughly corresponds to the probability content of 1,2 and 3 sigma, respectively. We recover the best value $M_* = -20.3$ for $D = 3$, found in Lin et al. (1996), but we see that, depending on α , essentially all values of D between 2 and 3 are allowed within two sigmas. For low α, a value $D = 2$ is actually the maximum likelihood estimator.

In Fig. 4.8 we show two best fit curves of $n(R)$, one with $D = 2$ and one with $D = 3$, compared with the data: in both cases the agreement is rather good (χ^2 /d.o.f.$\simeq 1$).

This is not to say that the data are fractal up to 625 Mpc/h. Rather, I want to show how difficult is to rule out the possibility that the distribution is fractal up to some large scale, and how the real fractal density scaling can modify the results of rather standard analyses. In the example above, a value of α much lower than the one commonly derived is consistent with the data if we allow for the density scaling. A lower value of α implies a relative abundance of bright galaxies. In other words, there is a degeneracy in the number count prediction between small α and D less than 3, because galaxies brighter on average compensate the decrease in density induce by a low fractal dimension.

Clearly, allowing for a fractal trend to, say,only 100 or 200 Mpc/h would require an even slighter modification of the value of α found for $D = 3$.

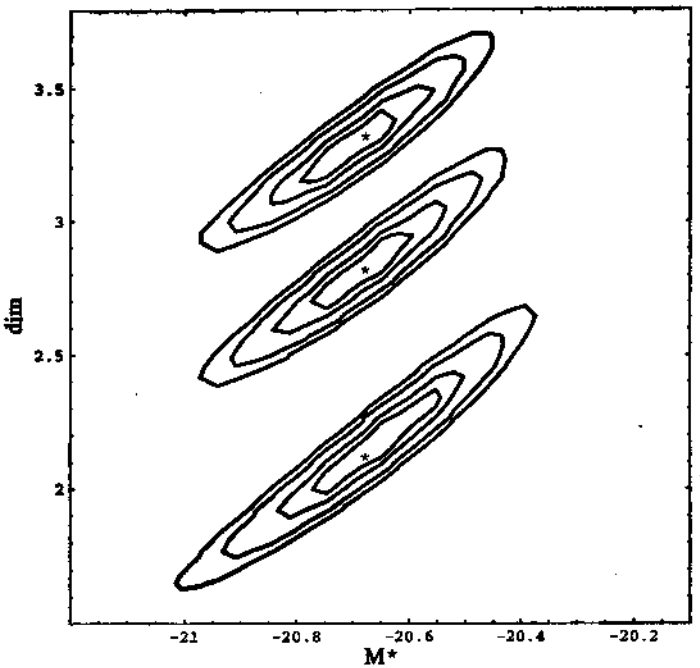

Figure 3.21: Likelihood contours on the plane M^*, D assuming $\alpha = -1.0, -0.7, -0.25$, top to bottom. The best fit dimension is $D = 2, 2.7, 3.3$, respectively.

3.4.7 Conclusions from the observations

The conclusions I can draw from the whole set of redshift catalogs are the following.

- Once we discard the tests based on amplitudes, because of the variance problem, we are left with only a few observations that can constrain the scale of homogeneity
- There is no doubt that a $D = 2$ fractal behavior up to 30 or 40 Mpc/h has been detected in many surveys, as expected even in standard CDM models
- The power spectra of CfA2, SSRS2 and LCRS are compatible both with fractals and with standard scenarios; the peak found in the spectra is not incompatible with the one a pure fractal would show in a finite sample
- The surveys CfA2 and SSRS2 are not deep enough to allow for the unambiguous test of the $\Gamma^*(r)$ to be performed, because the maximum cell that fits in is of the order of 50 Mpc/h, that is the same scale of fractality of CDM

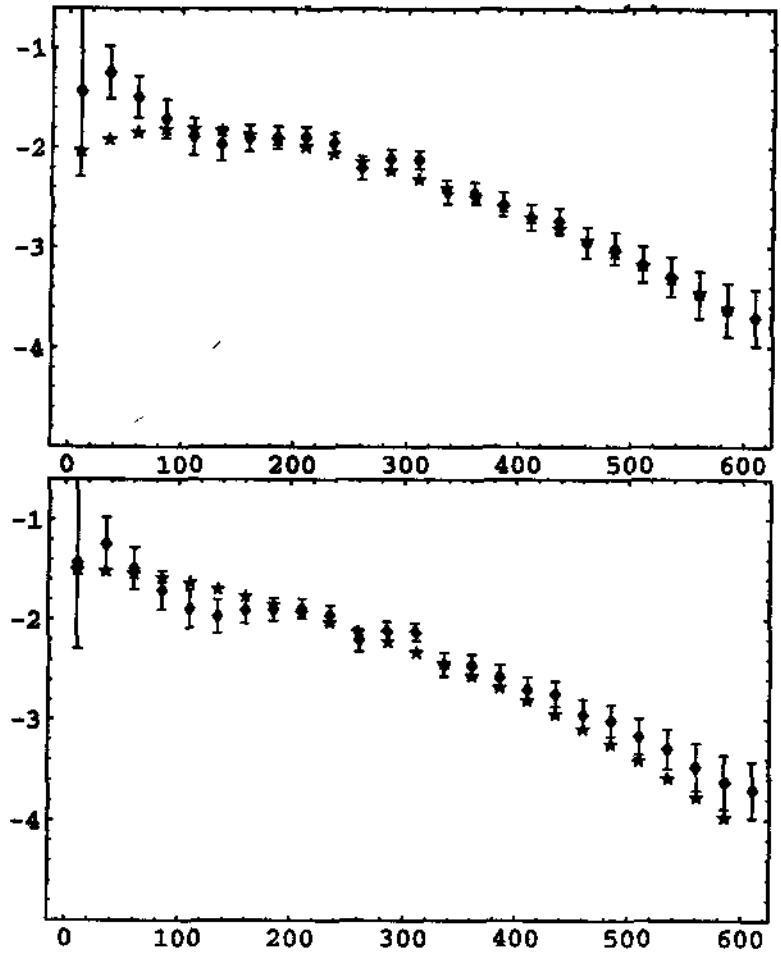

Figure 3.22: **Data from LCRS (symbols with errorbars) compared with the best fits for $\alpha = -0.25$ (top) and $\alpha = -0.7$ (bottom).**

- Only LCRS is deep enough to prove the crucial scales beyond 50 Mpc/h. In a preliminary analysis, we have found that the result is compatible with a $\sigma_8 = 1.5$ CDM with $\Gamma = 0.2$. A clear deviation from $D = 2$ toward $D = 3$ is found around 50 Mpc/h, but the plateau predicted in standard CDM around 100 Mpc/h is still not convincingly detected.

3.5 A model

3.5.1 Introduction to cosmological first order phase transitions

All what we have been saying so far can be summarized in one sentence: the level of inhomogeneities in our universe can be higher than usually assumed. The ultimate reason, as we have seen, is that any finite survey tends to underestimate the true inhomogeneities. Even a fractal extending to one or two hundreds of Megaparsecs cannot be excluded by observations of large scale structure alone. Now it is time to ask ourselves if such a high level of inhomogeneity can be produced in our universe without putting in jeopardy the cornerstones of standard cosmology.

Here we consider as cornerstones the inflationary mechanism for generating fluctuations and for solving the curvature and the horizon problems, and the observations of anisotropies in the microwave background. In these last Sections we will present a model of structure generation which does not challenge the cornerstones, but that produces strong inhomogeneities, in particular with a tendency to give a $D = 2$ distribution.

One of the most interesting ideas introduced in inflationary cosmology in recent years is the possibility of performing a phase transition *during* inflation. In such scenarios, two fields act on stage: one, say ω, slow rolls, driving enough inflation to solve the standard problems; the second field, say ψ, tunnels from a false vacuum state to an energetically favored true vacuum state, producing *bubbles* of the new phase embedded in the old one. Both processes are governed by a two-field potential $U(\omega, \psi)$ shown in Fig. 5.1.To avoid the graceful exit problem, the true vacuum state has to allow for a period of inflation on its own. We can then speak of a true vacuum *channel* over which the bubbles slow roll until inflation ends, and reheating takes over. Depending on the potential, three classes of first-order inflation models have been proposed so far. The first is the classical extended inflation (La & Steinhardt 1989): the bubbles are produced in a copious quantity, so that they eventually fill the space and complete the transition. To avoid too large distortions on the CMB, this scenario must produce very small bubbles (Liddle & Wands 1992), so that they are rapidly thermalized after inflation. No trace of the bubbles is left in our Universe, and from this point of view such scenarios do not lead to new predictions over inflation without bubble production. The second class is the $\Omega < 1$ inflation (Bucher, Goldhaber & Turok 1995; Linde 1995; Amendola, Baccigalupi & Occhionero 1996): here the transition is never completed, so that each bubble resembles an open Universe to inside observers. Therefore, if the bubbles inflate for less than the canonical $N_T = 60$ or so e-foldings, they will approach an $\Omega < 1$ Universe. Here the effect of the nucleation process

is observable, although it is indistinguishable from a slow roll inflation just shorter than N_T e-foldings and with no first-order phase transition at all. Finally, in Occhionero & Amendola (1994) a third class of models has been proposed, following an early suggestion of La (1991). In such models, the phase transition is completed *before* the end of inflation. Then, it has been shown that the primordial bubbles can be large enough to drive structure formation, and still be below the CMB level of detection. In such a scenario, the present large scale structure is a direct outcome of the first order transition, which is therefore observable and testable.

Several deep redshift surveys detected large voids in the galaxy distribution (see e.g. El-Ad, Piran & Da Costa 1996, 1997), although it is still not clear if they are really empty of matter or just lack luminous galaxies. Standard models of galaxy formation can account for these structure only at the price of adjusting the parameters to get very large scale power. If the voids are really empty of matter, as some observations suggest (Da Costa et al. 1996), and if their size continue to grow as deeper surveys are completed, it would be difficult to reconcile them with standard theories (Piran et al. 1993). Therefore, just as we associate matter clumps to primordial fluctuations, it appears worth trying to associate the present voids to primordial bubble-like fluctuations, produced during a first-order phase transition. Within different contexts, the idea of the voids as separate dynamical entities has been investigated several times in earlier literature (Ostriker & Cowie 1981).

A crucial aspect of bubble inflation is the calculation of the bubble spectrum $n_B(L)$, defined as the number of bubbles per horizon with comoving size larger than L. In Occhionero & Amendola (1994) we calculated n_B in a specific model, built on fourth order gravity (Starobinsky 1979), which we found to possess the requested features. We found that $n_B(L)$ can be approximated by a power law,

$$n_B = (L_m/L)^p\,, \tag{5.107}$$

and that L_m can be as large as the observed voids in the Universe.

The central quantity needed to evaluate n_B is the nucleation rate in the semiclassical limit (Coleman 1977)

$$\Gamma = \mathcal{M}^4 \exp(-B) \tag{5.108}$$

where $\mathcal{M}$ is a constant with a dimension of mass, and B is the Euclidean least action minus the action for the external deSitter spacetime solution. This calculation allows us to reconstruct completely the inflationary two-field potential from the determination of four observable quantities: the slope of the bubble spectrum, its amplitude, the density contrast inside the bubbles, and the amplitude of the ordinary slow-rolling fluctuations. We remark that only in a model, like ours, in which the bubbles are directly observable, it is possible to reconstruct the tunneling sector of the primordial potential.

We consider the scalar field theory described by the action (hereinafter, $\hbar = c = 1$)

$$S = \int d^4x\sqrt{-g}\left\{-\frac{\mathcal{R}}{16\pi G} + \frac{1}{2}\psi_{;\mu}\psi^{;\mu} - U(\psi)\right\} \tag{5.109}$$

where g is the metric determinant and $\mathcal{R}$ the curvature scalar. The potential is a generic quartic function with non-degenerate minima which allows for tunneling. We can write it very generally in the form

$$U(\psi) = \Lambda + V_1(\psi) + V_2(\psi) \tag{5.110}$$

where Λ is a cosmological constant, V_1 is a quartic with two equal-energy minima and V_2 is a symmetry-breaking potential which brings the energy of one minimum, the false vacuum (subscript F), to a value larger than the other, the true vacuum (subscript T). In the two minima, the Einstein equation reduces simply to

$$H^2 = 8\pi GU/3 \tag{5.111}$$

We will denote with H_T, U_T the Hubble constant and the potential energy of the true vacuum, and with H_F, U_F the same quantities for the false vacuum. We wish to calculate the tunneling rate (5.108) where $B = S_E(\psi) - S_E(\psi_F)$, and $S_E(\psi)$ is the Euclidean least action, i.e. the Action of the "bounce" solution. We perform the computation in the thin-wall limit, according to which the $O(4)$ bubbles nucleated have 4-radius $R \gg \Delta$, where Δ is the wall thickness. Further, we include the gravitational term in the action: as we will show, this term is important when the parameter $g = RH_T$ (not to be confused with the metric determinant) is much larger than unity. This limit amounts in fact to a bubble approaching the space curvature radius $1/H$. It is convenient to write the potential (5.110) in the form

$$U(\psi) = \frac{3g^2}{8\pi GR^2} + \frac{1}{2\Delta^2\psi_0^2}(\psi^2 - \psi_0^2)^2 + \frac{1}{R\Delta}(\psi + \psi_0)^2 \tag{5.112}$$

Then, the true vacuum state is $\psi = -\psi_0$, and the false vacuum is $\psi = \psi_0$ (Fig. 5.2). The potential (5.112) is therefore defined by four physical parameters: g, R, Δ, ψ_0.

The Euclidean action of the scalar theory (5.109) is

$$S_E = \int d^4x\sqrt{-g}\left\{-\frac{\mathcal{R}}{16\pi G} + \frac{1}{2}\psi_{;\mu}\psi^{;\mu} + U(\psi)\right\} \tag{5.113}$$

In the Euclidean metric for a O(4) space $ds^2 = dr^2 + a^2(r)d\Omega_3^2$ one has $\mathcal{R} = -6(aa'' + a'^2 - 1)/a^2$ and

$$S_E = 2\pi^2\int dr\left[\frac{3}{8\pi G}(a^2a'' + aa'^2 - a) + a^3(\frac{1}{2}\psi'^2 + U)\right] = -\frac{3\pi}{2G}\int dr\ a(1-a^2H^2) \tag{5.114}$$

where the prime denotes derivation with respect to the 4-radius r. The Euclidean Klein-Gordon equation for ψ is

$$\psi'' + 3\frac{a'}{a}\psi' = dU/d\psi \tag{5.115}$$

and the Euclidean Friedmann equation is

$$a'^2 = 1 + \frac{8\pi G}{3} a^2 (\frac{1}{2}\psi'^2 - U) \tag{5.116}$$

In the zero-gravity limit, $G \to 0$, the latter equation gives $a' = \text{const}$, so that (5.115) reduces to

$$\psi'' + \frac{3}{r}\psi' = dU/d\psi \tag{5.117}$$

In the thin-wall limit, in which $R \gg \Delta$, one can assume that the second term in (5.117) can be neglected, and that $dU/d\psi = 2\psi(\psi^2/\psi_0^2 - 1)/\Delta^2$. The solution which interpolates between false and true vacuum is then

$$\psi^{(0)} = \psi_0 \tanh\left(\frac{r - R_w}{\Delta}\right) \tag{5.118}$$

where R_w is an integration constant that will be determined later. To integrate the action over the bounce solution, we consider that outside the bubble, i.e. in the false vacuum, $\psi = \psi_0$, so that $B_{ext} = S_E(\psi_0) - S_E(\psi_0) = 0$. On the wall, at distance R_w, we have $B_{wall} = 2\pi^2 R_w^3 S_1$ where

$$S_1 = \int_{-\psi_0}^{\psi_0} d\psi \, [2(U(\psi) - U_F]^{1/2} = \frac{4\psi_0^2}{3\Delta} \tag{5.119}$$

Finally, inside the bubble, $\psi = -\psi_0$, and since (from (5.116), and neglecting ψ') $da = dr\,[1 - a^2 H_T^2]^{1/2}$ we have

$$B_{int} = -\frac{3\pi}{2G} \int_0^{R_w} a da \left[(1 - a^2 H_T^2)^{1/2} - (1 - a^2 H_F^2)^{1/2}\right] \tag{5.120}$$

The general expression is therefore

$$B(R_w) = 2\pi^2 R_w^3 S_1 + \frac{\pi}{2G}\left\{H_T^{-2}\left[(1 - R_w^2 H_T^2)^{3/2} - 1\right] - H_F^{-2}\left[(1 - R_w^2 H_F^2)^{3/2} - 1\right]\right\} \tag{5.121}$$

Let us note that $R = 3S_1/\varepsilon$, where $\varepsilon = U_F - U_T = 4\psi_0^2/R\Delta$. Then we see that $B(R_w)$ is minimized by (Parke 1983)

$$R_w = R\left(1 + g^2 + 4\pi G R S_1 + 12\pi^2 G^2 R^2 S_1^2\right)^{-1/2} \tag{5.122}$$

Then, for $G \to 0$, which implies $g = RH_T \to 0$, one has $R_w = R$. Notice that the parameter $R_w H_T$ which appears in (5.121) equals g, since $H_T^2 = g^2/R^2$ for the potential (5.112). This shows explicitly the role played by the constants R

and g. Finally, we obtain the usual (zero-gravity, thin-wall) result (Coleman 1977)

$$B_0 = 27\pi^2 \frac{S_1^4}{2\varepsilon^3} = \frac{2\pi^2}{3} \frac{R^3 \psi_o^2}{\Delta} \tag{5.123}$$

In the general case, $G \neq 0$, and assuming $(H_F^2 - H_T^2)/H_T^2 \ll 1$, i.e. that the vacuum energy difference is much smaller than the true vacuum energy, we get $B = B_0 f(g)$ where B_0 is the no-gravity action (5.123) and where

$$f(g) = 4(1+g^2)^{-3/2} \left\{ 1 + g^{-4}[2 + 3g^2 - 2(1+g^2)^{3/2}] \right\} \tag{5.124}$$

For $g \to 0$, $f(g) \to 1$, as expected. To the lowest non-trivial order in g,

$$B = B_0(1 - g^2) \tag{5.125}$$

Gravitational effects, then, increase the nucleation rate Γ (Callan & Coleman 1977).

Finally, we can express the tunneling rate in the post-thin-wall approximation (Amendola et al. 1996). The Euclidean action turns out to be

$$B = B_0(1 - 9\Delta/2R) \tag{5.126}$$

The post-thin-wall correction term again increases the tunneling rate. Combining Eq. (5.123), Eq. (5.126) and Eq. (5.125), we obtain

$$B = \frac{2\pi^2}{3} \frac{R^3 \psi_0^2}{\Delta} \left(1 - \frac{9\Delta}{2R} \right) (1 - g^2) \tag{5.127}$$

To get a tunneling rate which depends on the nucleation time, we now assume that R and g depends on the nucleation e-folding time N as a simple power-law

$$g \sim R \sim N^\alpha \tag{5.128}$$

with $\alpha > 0$. This behavior is motivated by the simple physical model investigated in Amendola et al. (1996), based on fourth order gravity, but is general enough to cover a variety of cases. Then the bounce action is

$$B(N) = \left(\frac{N}{N_1} \right)^{3\alpha} \left[1 - \left(\frac{N}{N_2} \right)^{-\alpha} \right] \left[1 - \left(\frac{N}{N_3} \right)^{2\alpha} \right] \tag{5.129}$$

where the constants N_1, N_2, N_3 are defined in terms of the potential parameters Δ, ψ_0 and of the normalization of $R(N)$ and $g(N)$. The approximations we have made are then valid if $N > N_2$ (post-thin-wall limit) and $N < N_3$ (gravitational correction). If these conditions are fulfilled, we can write $B(N) \simeq \beta(N/N_1)^{3\alpha}$, with β a slowly varying function of N of order

unity. We also impose the condition that $N > N_1$ in order that the semiclassical approximations are valid.

We can now calculate explicitly the bubble spectrum in our model. The number of bubbles nucleated in the interval dt is

$$\frac{dn_B}{dt} = \Gamma a^3 V_{in} \exp(-I), \quad I \equiv \left\{ -\frac{4\pi}{3} \int_0^t dt' \Gamma(t') a^3(t') \left(\int_{t'}^t \frac{d\tau}{a(\tau)} \right)^3 \right\}, \quad (5.130)$$

where V_{in} is the horizon volume at $N = N_T$, $V_{in} = 4\pi/3H_{in}^3$, and where the exponential factor accounts for the fraction of space which remains in the false vacuum. To get a manageable expression, we first change variable in Eq. (5.130) from the nucleation epoch t to the scale L in horizon-crossing at t, by use of the relation $dL/dt \approx -H_{in}L_h/a$ valid during slow roll. This gives

$$\frac{dn_B}{dL} = -3L_h^3 L^{-4} Q(N) e^{-I}. \quad (5.131)$$

where the dimensionless tunneling rate Q can be written as

$$Q = \frac{4\pi\Gamma}{9H^4} = \exp[B(N_0) - B(N)] \quad (5.132)$$

Here, the constant N_0 denotes the instant at which $Q = 1$. After this stage, the nucleation can be considered over, because more than one bubble per horizon volume per horizon time is nucleated. Approximating $Q(N)$ around $N = N_0$ as $Q \approx \exp[s(N_0 - N)]$, we obtain

$$s = (dB/dN)_0 = 3\alpha\beta(N_0/N_1)^{3\alpha}/N_0 \quad (5.133)$$

Making use of the relation between the e-folding time N and the bubble comoving size L, $HL(N) = H_{in}L_h \exp(N - N_T)$. It follows $Q = e^{-s\Delta N}(L_h/L)^s$, where $\Delta N = N_T - N_0$ corresponds to the duration of the transition. For $I \ll 1$, i.e. far from the end of the transition, we obtain, as anticipated, a power-law spectrum of bubbles

$$n_B = (L_m/L)^p, \quad p = 3 + s \quad (5.134)$$

where

$$L_m = L_h e^{(3-p)\Delta N/p} (3/p)^{1/p} \quad (5.135)$$

The precise value of s depends on the specific model. For instance, in Occhionero & Amendola (1994) we considered a model with s of order unity. The slope p and the amplitude L_m are therefore the observable quantities that depend on the potential parameters mainly through N_0 and N_1.

When I approaches unity, the nucleation process reaches a peak, and then declines rapidly, due to the fast decrease in the false vacuum space available. In Occhionero & Amendola (1994) we showed that the peak occurs, as expected, just after N_0, which we therefore consider the end of the nucleation.

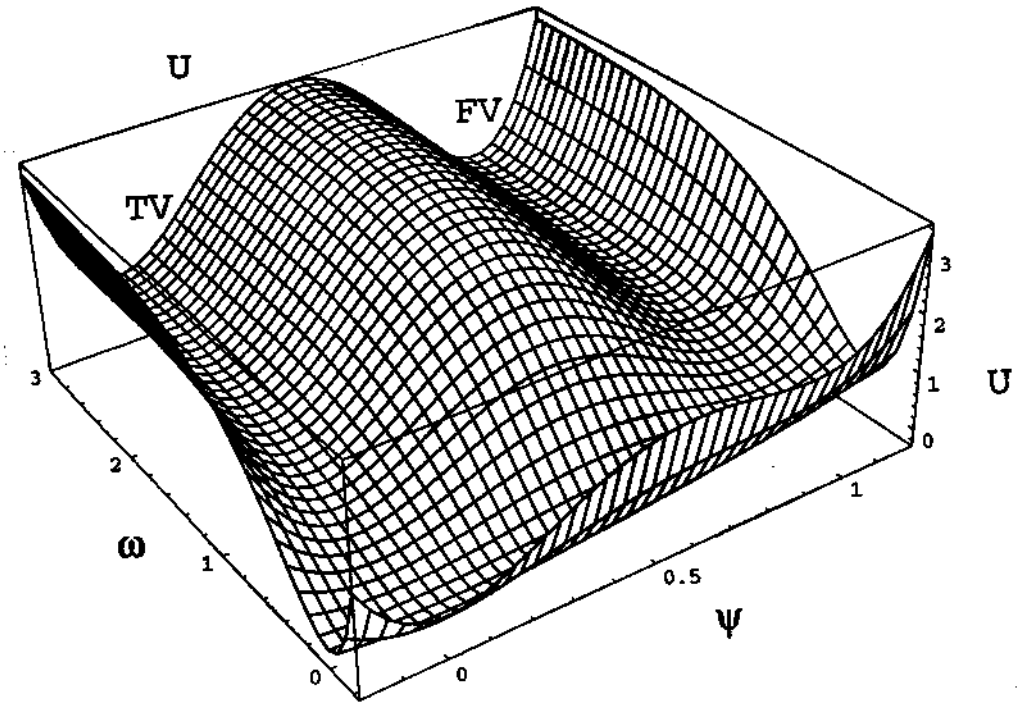

Figure 3.23: **Two-dimensional potential with tunneling (along ψ) and slow-rolling (along ω).**

3.5.2 Constraints on the bubble spectrum

The bubbles so produced have a distribution of $\delta\rho/\rho$ which reflects the initial energy contrast between the false and true vacuum. They expand comovingly at first, then reenter the horizon, and in the matter dominated era expand slightly overcomovingly (Occhionero et al. 1997). Depending on the initial density contrast they can be either empty by today or contain some matter density. They can also reach shell-crossing during the evolution and form structure on the shells, again depending on the initial density contrast and density profile (Occhionero et al. 1997).

In Fig. 5.2 we show that a distribution of voids that can be fitted by the power law (5.134) does indeed provide large scale power (Fiorentino 1997). Roughly speaking, a distribution filling a major fraction of space with bubbles extending to radius R give fractality with $D \simeq 2$ up to $\lambda_h = 2R$. Since the bubbles grow by an overcomoving factor of 2 from decoupling to now, bubbles of size R at decoupling give fractality up to $4R$ by the present time. As a consequence, if bubbles of radius e.g. 25 Mpc/h are acceptable for as concerns their signal on the microwave background, they can produce fractality up to 100 Mpc/h. This is what will be shown below.

To evaluate the constraints on the microwave background we can work in two limits: empty, non-linear bubbles, and linear bubbles. The first case has been solved so far only considering the Sachs-Wolfe effect (Baccigalupi et al. 1997). Here we focus on the linear case (Amendola, Baccigalupi & Occhionero 1998) in which the full calculation is possible.

We consider for simplicity a class of interesting bubble model which are likely not to give too strong anisotropies, but still produce relevant inhomogeneities by today. We assume then that the voids are today from 20 to 60 Mpc/h by radius, as suggested by some observations. Because the voids had a slight overcomoving growth, they were around 10 to 30 Mpc/h at decoupling (Occhionero et al. 1997). To further simplify the matter, we consider voids of constant radius, either of R =10, 20 or 30 Mpc/h at decoupling. The number of voids is deduced by the requirement that *today* they fill a fraction X of the space; we take $X = 50\%$, consistently with, e.g., El-Ad et al. (1996) and explore also values from 10 to 70 %. The central density contrast at decoupling δ is a free parameter in our model, and we consider values in the range $\delta \in (.001 - .1)$, so that the linear approximation can be employed to evaluate the radiation anisotropy ($\delta < 0.1$), and the voids become empty by the present time ($\delta > 0.001$). Each of our distributions is therefore parametrized by three numbers, the radius R, the filling fraction X, and the central density contrast δ. It is important to remark that each set of parameters we adopt in this paper can be obtained in the primordial potentials seen above. The features we are going to describe on the CMB maps put therefore direct constraints on the inflationary model.

To create the maps, we distribute the voids randomly near the last scattering surface, i.e. in a shell of size $2R$ centered on the surface. Voids much farther than this from the scattering surface give a negligible contribute. As explained next, we calculate for each void the radiation anisotropy field $\Delta T/T$, taking into account the Sachs-Wolfe effect (the integrated Sachs-Wolfe effect being negligible), the Doppler mechanism, the adiabatic coupling. Once we have the $\Delta T/T(\theta)$ for any void, where θ is the angular distance from the void center, we build maps of standard CDM fluctuations plus voids. The voids are distributed randomly because their filling factor *at nucleation* is small enough to consider each nucleation independently of the other nucleations. The CMB anisotropy field induced by linear bubbles has been computed in detail in Baccigalupi (1998). Since our bubbles are linear, we can use the standard procedure of solution of the photon-baryon-dark matter fluid. Briefly, a bubbly perturbation at reheating is modelled analytically and Fourier transformed. By using the theory of linear perturbations (we employed the formulation proposed by Hu & Sugiyama 1995) in a standard cosmological scenario ($\Omega_0 = 1, \Omega_b = 0.06, h = 0.5, \Lambda = 0$, COBE normalization $Q^{PS}_{rms} = 18\mu$K), the corresponding perturbation modes in the photon-baryon plasma are evolved until decoupling, when they generates CMB anisotropies. For an isolated bubble, the anisotropy pattern is composed of a central (adiabatic and Sachs-Wolfe) spot and a series of acoustic waves which give rise to concentric isothermal rings of alternate sign of $\Delta T/T$ (*Doppler rings*) on the scale of the sound horizon at decoupling ,$\leq 1^o$ in the sky. The mean amplitude of the central

spot follows the expected trend for linear perturbations, $\Delta T/T \simeq \delta(R/H^{-1})^2$. As noticed above, the $\Delta T/T$ scales roughly as $R^2\delta$, so that we expect the total effect *of a single bubble* on the radiation anisotropy field to depend, to a good approximation, on this product alone.

The void size corresponds on the decoupling surface to a spot of R/L_h radians, where $L_h = 6000\text{Mpc}/h$ is the horizon radius; this angular size is therefore from 6 to 18 arcmin. We expand, as customary, the map $\Delta T/T(\theta,\varphi)$ in spherical harmonics $\Delta T/T(\theta,\varphi) = \sum_{\ell m} a_{\ell m} Y_m^\ell(\theta,\varphi)$, and calculate the angular power spectrum

$$C_\ell = \sum_m |a_{\ell m}|^2/(2\ell+1).$$

As an angular size of $\sim$10 arcmin corresponds to $\ell \approx 1000$, we expect an increase in power at this multipole order for $R = 10 - 20h^{-1}$Mpc, and at smaller ℓ for larger R.

We show in Fig. 5.3 three $6^0 \times 6^0$ maps of the CMB for various values of R, X and δ. For each set of parameters we plot in Fig. 5.4 the C_ℓ spectrum. For $R = 10$ and 20 h^{-1}Mpc, a clear feature of the angular power spectra is that the first Doppler peak of the CDM distribution is left almost unperturbed by the primordial voids, while for large δ a *second prominent peak* appears at $\ell_{peak} \approx 1000$ as expected (Fig. 5.4). For $R = 10h^{-1}$Mpc the peak structure shows a broad top ($\ell \in (800, 1500)$), with a secondary peak at larger ℓ. For $R = 20h^{-1}$Mpc the peak becomes sharper, and it moves at $\ell \approx 700$. Finally, for $R = 30h^{-1}$Mpc the peak is at $\ell \approx 400$, so that it overlaps with the CDM first peak. The peak is a clear diagnostics of the void model, being strongly dependent on R, X and δ.

For each value of R there is a value of δ below which the voids power is dominated by the CDM power; for instance, $\delta \approx 2\%$ if $R = 10$ Mpc/h. This means that a power spectrum analysis cannot detect these shallow bubbles, although they might be detected by their non-Gaussian features. The most important consequence is that there are models of primordial voids (plus CDM) that, although indistinguishable from pure CDM for as concerns the CMB angular spectrum, do contribute very significantly to structure formation. In fact, the voids considered here fill, as mentioned, 50% of the space today, and are underdense enough ($\delta \geq .001$) to develop completely empty void by the present time. In other words, finding a CDM spectrum on the microwave background does not rule out the possibility that today's galaxy distribution is shaped to a large extent by the primordial voids.

We are now in position to predict the angular spectrum in our voids-plus-CDM model, to compare with the next generation experiments on the CMB. The simplest prediction is the height of the second peak in the spectrum. Since the bubbles induce an *extra* power in C_ℓ, we found easier to model not the peak height itself, but rather the difference in power between the CDM+bubbles model , C_{tot}, and the CDM alone C_{cdm}, at the location ℓ_{peak} of the peak. This quantity expresses directly the extra power induced by the bubbles. Let us denote this quantity as the bubble peak power $C_{peak} = C_{tot} - C_{cdm}$. We

found an empirical relation between $\tilde{C}_{peak} \equiv [\ell(\ell+1)C_{peak}/(2\pi)]^{1/2}$ and R (in Mpc/h) and δ at constant X:

$$\tilde{C}_{peak} \approx \tilde{C}_0 (R/10h^{-1}\mathrm{Mpc})^{3.4}\delta \tag{5.136}$$

where $\tilde{C}_0 \approx 1.1\mathrm{m\ K}$. For $R \approx 10 - 20h^{-1}$Mpc, the total power at ℓ_{peak} is roughly $\tilde{C}_{peak} + 50\mu$K. For instance, a peak $\tilde{C}_{peak} = 100\mu$K implies $\delta \approx 0.1$ at decoupling if we require the voids to be 20 Mpc/h today by radius, and therefore $R = 10$ Mpc/h at decoupling. We also found that the dependence on X is linear in the range $X = 10 - 70\%$. Finally, the location of the peak is , as expected, $\ell_{peak} \approx 1200(10h^{-1}\mathrm{Mpc}/R)$, although, as we have seen, for small R the peak structure is not simple, due to the large number of bubbles to get $X = 50\%$.

In a panel of Fig. 5.4 we also show the variance for different realization of the CMB sky, corresponding to different random distributions of voids; this variance is due to the voids alone, the CDM realization being fixed. This effect is therefore to be added to the cosmic variance. In the same panel, we also show the effect on the peak of assuming different values for X.

Current observations focused so far on the first Doppler peak around $\ell = 200$. The data at higher ℓ are very uncertain. If we take the results by Scott et al. (1996) from the CAT experiment, $\tilde{C}_{\ell=590} = (48^{+20}_{-15})\mu$K, then we can "exclude" at the 1σ confidence level the values $\delta \geq .002$ for $R = 30h^{-1}$Mpc, $\delta \geq .01$ for $R = 20$ Mpc/h , and $\delta \geq .1$ for $R = 10$ Mpc/h. As a consequence, voids larger that $30h^{-1}$Mpc at decoupling with $X = 50\%$ can hardly be empty by today. We observe in passing that voids of size $40\,h^{-1}$Mpc produce power on the same scale of the CDM first peak, so that they could be invoked to explain some experiments at $\ell \approx 200$ showing more power than predicted by standard CDM. Other published data are either at much higher multipole order than our peaks, or are less stringent than the CAT data (see e.g. the compilation in Tegmark 1998). The resolution requested for voids larger than $10\,h^{-1}$Mpc is at least $\ell = 1000$; also, a map of several square degrees is necessary to distinguish the non-Gaussian features of the void temperature profile. In the near future, experiments as Boomerang and CAT will be able to produce maps with this resolution, and with adequate sensitivity; also OVRO, WD and SuZIE can put interesting constraints on our model (updated references in Tegmark 1997). The proposed Planck satellite will be of course particularly suitable, while MAP is favorable only for $R \geq 25h^{-1}$Mpc.

Of course, the CMB maps can be investigated through phase-independent statistics, like the angular power spectrum, or by methods which are sensitive to the phases, like wavelet transform and other non-Gaussian techniques (see e.g. Amendola 1996; Ferreira & Maguejo 1997). Here we confined ourselves to the angular power spectrum, by far the most popular statistics in the CMB field.

Consider now Eq. (5.136). Let us assume a distribution of voids of 25 Mpc/h by radius, which give fractality up to 100 Mpc/h by today. If they have $\delta = 0.001$ at decoupling, so that they are empty by today by linear growth, produce an extra peak of 25 μK at $\ell \simeq 500$, to be added to the

Gaussian fluctuations. This is perfectly compatible with current constraints on the microwave background. If δ is assumed smaller, so that the voids are not completely empty by today, then even larger voids can be produced. It is clear that these considerations are very rough, and that a more accurate study of the parameter space is necessary in order to put precise constraints on the maximum scale of homogeneity from bubbles. Nevertheless, this shows that a simple extension of the standard scenario of structure formation can produce much stronger inhomogeneity than usually assumed.

To summarize, the results of this section are *a*), the voids induce a well-defined second peak around $\ell = 1000$ in the C_ℓ spectrum for $R \leq 20h^{-1}$Mpc; *b*), there is a direct relation between the height of the second peak in the C_ℓ spectrum and the void parameters R, X and δ; *c*), there are distribution of voids that, although indistinguishable from standard CDM regarding the CMB angular spectrum, still produce significant large scale structure, as required by current redshift surveys; and *d*), an homogeneity scale of order 100 Mpc/h at the present can be obtained without breaking the CMB constraints. Our predictions can be compared to the results of the next generation high-resolution experiments on the CMB.

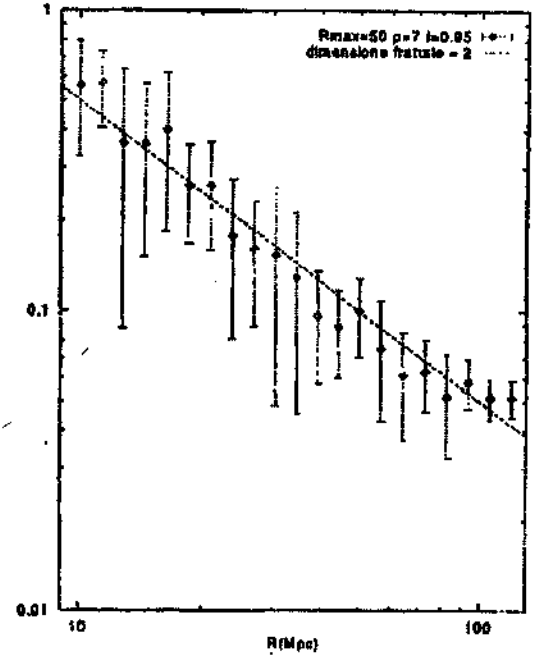

Figure 3.24: **Conditional density $\Gamma^*(r)$ for a distribution of voids with maximum radius $R = 50$ Mpc/h. There is $D \simeq 2$ fractality up to 100 Mpc/h.**

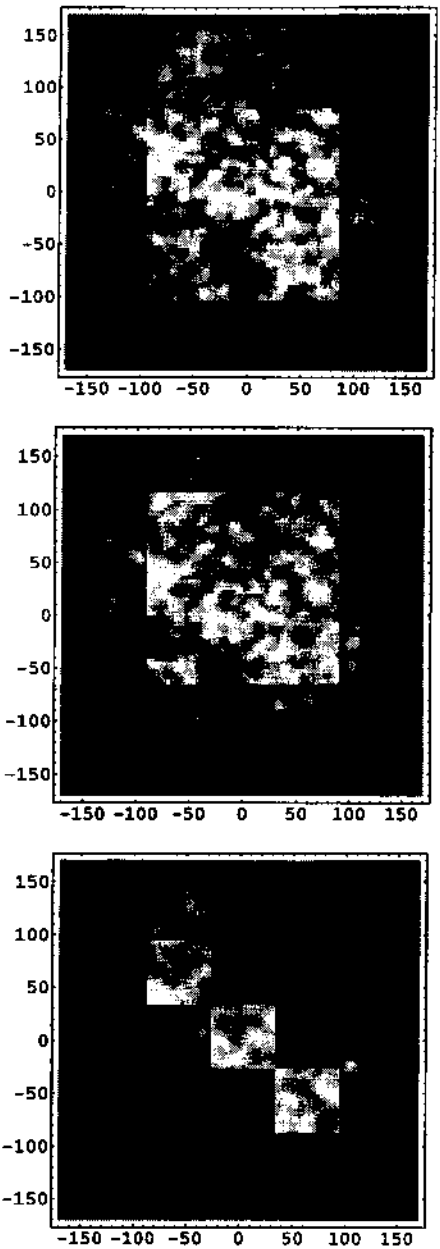

Figure 3.25: **Maps of CMB, 6 degrees by side, resolution 5 arcmin. Top: Standard CDM plus voids with $R = 10$ Mpc/h, $X = 50\%$, and $\delta = 0.07\%$. Center: as above, with $\delta = 0.05$. Bottom: as above, with $\delta = 0.01\%$. The C_ℓ spectra are reported in the next figure.**

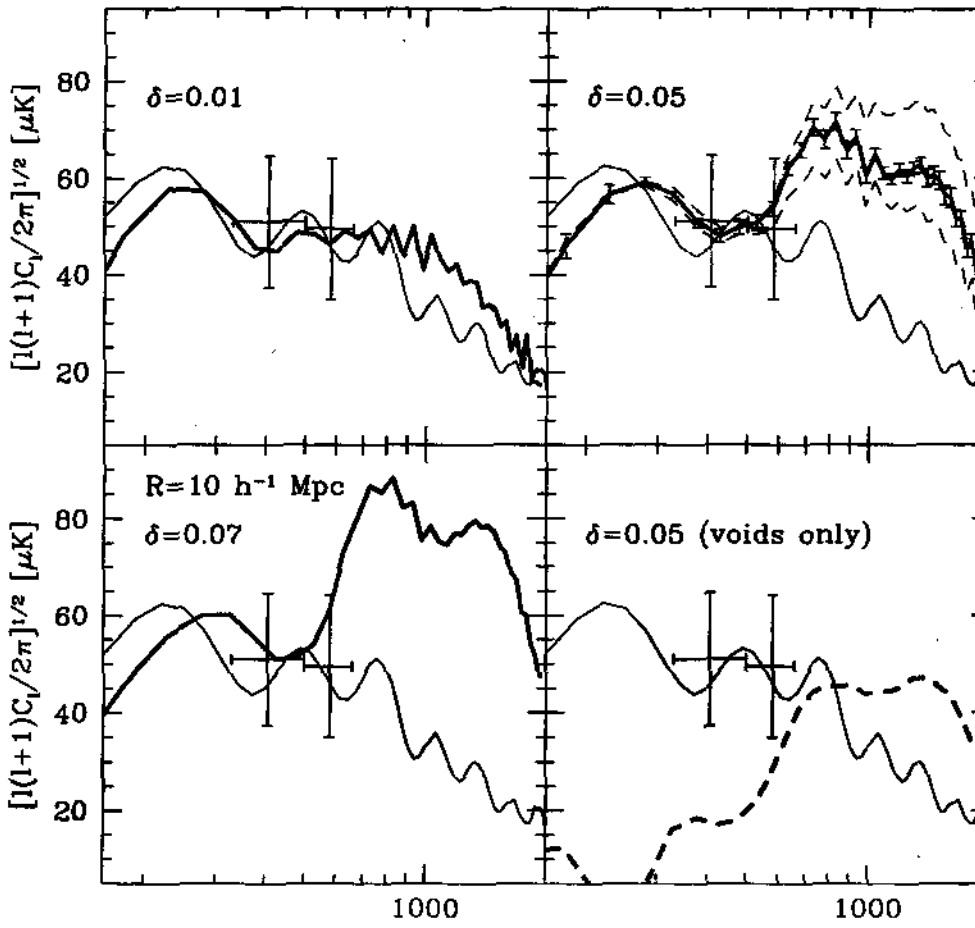

Figure 3.26: **Angular power spectra of CMB fluctuations in models of voids plus CDM with the parameters indicated and $X = 50\%$. In all the panel, the thin line shows the theoretical CDM spectrum. While the first peak is left almost unperturbed, the voids induce a second peak at large ℓ. The larger R, X and δ, the higher the peak. The crosses are the CAT results by Scott et al. (1996). In the top right panel we plot also C_ℓ for $X = 30\%$ (lower dotted line) and $X = 70\%$ (top dotted line) (see text). In the same panel we put the errorbars, as explained in the text. In the bottom right panel we plot the pure void contribution (dashed line) with $R = 10$ Mpc$/h$ and $\delta = .05$.**

3.6 Acknowledgments

Many thanks to Prof. Mario Novello for the invitation to the IX Brasilian School of Cosmology and Gravitation, that provided me the opportunity to review the topics collected here. I also acknowledge many insightful discussions with C. Baccigalupi, H. Di Nella, M. Fiorentino, M. Joyce, M. Montuori, E. Palladino, L. Pietronero, F. Occhionero, F. Sylos-Labini.

3.7 References

Amendola L., 1994, Ap. J., 430, L9

Amendola L. 1996, MNRAS, 283, 983

Amendola L. 1997, MNRAS, 290, 59

Amendola L. & Occhionero F., 1993 Ap. J. 413, 39

Amendola L., Baccigalupi C., & Occhionero F., 1996, Phys. Rev. D, 54, 4760

Amendola L., Baccigalupi C., & Occhionero F., 1998, Ap. J., 492, L5

Amendola L., Baccigalupi C., Konoplich R., Occhionero F., Rubin S., 1996, Phys. Rev. D54, 7199

Amendola L. & S. Borgani, 1994, MNRAS. 266, 191

Amendola L, Di Nella H., Montuori M., Sylos-Labini F., 1997, Fractals, 5, 635

Baccigalupi C., 1997, Ap. J., 496, 615

Baccigalupi C., Amendola L. & Occhionero F. 1997, MNRAS 288, 387

Baccigalupi C., Amendola L. , Fortini P. & Occhionero F., 1997, Phys. Rev. D56, 4610

Balian R. & Schaeffer R., Ap. J., 335, L43 (1988)

Baryshev, Y., Sylos Labini, F., Montuori, M., Pietronero, L. Vistas in Astron. 1994, 38, 419

Baugh C.M. and Efstathiou G. MNRAS,, 267 (1994) 323

Bennett C.L. et al., Ap.J., 436 (1994), 423

Benoist C., Maurogordato S., Da Costa L.N., Cappi A., and Schaeffer R., 1996, Ap. J.,472, 452

Bond, J.R. & Efstathiou, G., MNRAS , 226, 655

Borgani S., 1995, Phys. Rep., 251, 1

Bucher M. , A.S. Goldhaber, & N. Turok, Phys. Rev. D 52 3314 (1995);

Callan C. and S. Coleman, Phys. Rev. D , 16 1762 (1977);

Cappi A., Benoist C., Da Costa L.N., Maurogordato S., 1998, astro-ph/9804085

Coleman, S., Phys. Rev. D, 2929 (1977);

Coleman S. and F. De Luccia,1980 , Phys. Rev. D, 21, 3305 .

Coleman, P.H. Pietronero, L.,& Sanders,R.H., Astron. Ap. Lett. 245, (1988), 1

Coleman, P.H. & Pietronero, L., Phys.Rep. 231, (1992) 311

Da Costa, L. N. *et al.* Ap. J., 327, (1988) 544

Da Costa L.N., Freudling W., Wegner G., Giovanelli R., Haynes M. & Salzer J.J, 1996, Ap. J., 468, L5
Da Costa, L. N. *et al.* Ap. J. 424, (1994) L1
Da Costa L.N., Vogeley, M., Geller, M.J., Huchra, J., Park, C., 1994, ApJ 437,L1
de Vaucouleurs G., 1970, Science 167, 1203
Di Nella, H., Montuori M., Paturel, G., Sylos Labini, F., & Pietronero L. 1996, A&A Letter, 308, L33.
El-Ad H., Piran T. & Da Costa L.N., 1996 Ap. J. 462, L13
El-Ad H., Piran T. & Da Costa L.N., 1997, MNRAS 287, 790
Feldman H. A., Kaiser, N., & Peacock, J.A. 1994, Ap. J., 426, 23
Ferreira P. , Maguejo J., 1997, Phys. Rev. D55, 3358
Fiorentino M. 1997, Thesis, Univ. of Rome, unpublished
Fisher K.B., Davis, M., Strauss, M., Yahil, A., & Huchra, J.P., 1993, ApJ 402, 42
Gaztanaga E., 1994, MNRAS, 268, 913
Gaztanaga E., Croft R. A. & Dalton G. B., 1995, MNRAS, 276, 336
Guth A. and E.J. Weinberg, Nucl. Phys. B212, 321 (1983)
Hu W. & Sugiyama N. 1995 Ap. J. 444, 489
Juszkiewicz R., Bouchet F. & Colombi S., 1993, Ap. J., 412, L9
Kirshner R.P., Oemler A., Schechter P.L., Shectman S.A., 1981, ApJ 248, L57
Kosowsky A. & Turner M. S. 1993 Phys. Rev. D47, 4372
La D. 1991, Phys. Lett. B265, 232
La D. & Steinhardt P. 1989 Phys. Rev. Lett. 62, 376
Landy S. D. , S.A. Schectman, H. Lin, R.P. Kirshner, Oemler A.A., & D. Tucker, Ap. J., 456, L1 (1996)
Liddle A.R. and D. Wands, MNRAS 253, 637 (1991).
Lin H., et al. 1996a, ApJ , 464, 60
Lin H. et al. 1996b, Ap. J., 471, 617
Linde A. , Phys. Lett. B351 99 (1995);
Loveday J.*et al.* 1995 Ap. J., 442, 457
Maddox *et al.*, 1990, MNRAS, 242, 43
Mandelbrot B., (1982) The Fractal Geometry of Nature, Freeman, New York
Occhionero F. & Amendola L., 1994, Phys. Rev. D50, 4846
Occhionero F. , Baccigalupi C., Amendola L. & Monastra S., 1997, Phys. Rev. D , 56, 7588
Ostriker J.P. and L.N. Cowie, Ap. J. 243, L127 (1981);
Padmanabhan T., Structure Formation in the Universe, 1993, Cambridge Univ. Press
Paladin G. & Vulpiani A., 1987, Phys. Rep. 156, 147
Palladino E., 1997, Thesis, Univ. of Rome, unpublished
Park, C., Vogeley, M.S., Geller, M., Huchra, J. Ap. J., 431, (1994) 569
Parke,S. Phys. Lett. 121B, 313 (1983)
Paturel, G., Bottinelli, L., Gouguenheim, L., 1994 , Astron. Ap., 286, 768
Peacock J. A. & Dodds S. J., 1994, MNRAS 267, 1020
Peacock, J.A., Nicholson, D. MNRAS 235, (1991) 307

Peebles, P. J. E. Large Scale Structure of the Universe , 1980, Princeton Univ. Press
Peebles P. J. E.,Principles of Physical Cosmology, 1993, Princeton Univ. Press
Pietronero L., Physica A, 144, (1987) 257
Pietronero L., Montuori M., Sylos Labini F., in the Proc of the Conference "Critical Dialogues in Cosmology" N. Turok Ed. (1997) World Scientific
Piran T., Lecar M., Goldwirth D., Da Costa L.,Blumenthal G.,1993 MNRAS,265,681
Schechter, P., (1976) Ap.J. 203,297
Scott P. F. et al., 1996, Ap. J. 461, L1
Starobinsky A.A. , Sov. Phys. JETP Letters, 30, 682 (1979).
Starobinsky A.A. , Sov. Astron. Lett. 9(5), 302 (1983).
Stocke J. *et al.* Ap. J. 451, 24 (1995);
Strauss M.A., *et al.*, Ap.J.Suppl. 83, (1992) 29
Sylos Labini, F. Amendola, L. Ap.J., 468, (1996) L1
Sylos Labini F., Montuori M., Pietronero L., 1996, Physica A, 230, 336
Sylos Labini F., Montuori M., Pietronero L., 1998, Physics Report, 293, 61
Sylos Labini F. & Pietronero L., 1996, Ap.J., 469 , 26
Sylos Labini F., Gabrielli A., Montuori M., Pietronero L., 1996, Physica A, 226, 195
Szomoru A. *et al.* AJ 108, 491 (1994)
Yoshioka S. and S. Ikeuchi, Ap.J. 341, 16 (1989);
Tadros H., & Efstathiou G., 1996, MNRAS , 276, L45
Tegmark M. , 1998, data collected in www.sns.ias.edu/~max/cmb/'experiments.html
Tucker D.L. *et al.*, 1997, MNRAS 285, 5
Van de Weygaert R. and V. Icke, Astron. & Astroph. 213, 1 (1989).
White S.D., Efstathiou G. & Frenk C.S., 1993, MNRAS 262, 1023
Zaroubi S. et al. 1997, Ap.J., 486, 21